NASA/TM-2004-212991

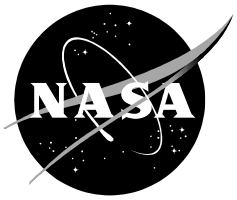

Wind Tunnel Application of a Pressure-Sensitive Paint Technique to a Faceted Missile Model at Subsonic and Transonic Speeds

Gary E. Erickson
Langley Research Center, Hampton, Virginia

February 2004

The NASA STI Program Office ... in Profile

Since its founding, NASA has been dedicated to the advancement of aeronautics and space science. The NASA Scientific and Technical Information (STI) Program Office plays a key part in helping NASA maintain this important role.

The NASA STI Program Office is operated by Langley Research Center, the lead center for NASA's scientific and technical information. The NASA STI Program Office provides access to the NASA STI Database, the largest collection of aeronautical and space science STI in the world. The Program Office is also NASA's institutional mechanism for disseminating the results of its research and development activities. These results are published by NASA in the NASA STI Report Series, which includes the following report types:

- TECHNICAL PUBLICATION. Reports of completed research or a major significant phase of research that present the results of NASA programs and include extensive data or theoretical analysis. Includes compilations of significant scientific and technical data and information deemed to be of continuing reference value. NASA counterpart of peer-reviewed formal professional papers, but having less stringent limitations on manuscript length and extent of graphic presentations.

- TECHNICAL MEMORANDUM. Scientific and technical findings that are preliminary or of specialized interest, e.g., quick release reports, working papers, and bibliographies that contain minimal annotation. Does not contain extensive analysis.

- CONTRACTOR REPORT. Scientific and technical findings by NASA-sponsored contractors and grantees.

- CONFERENCE PUBLICATION. Collected papers from scientific and technical conferences, symposia, seminars, or other meetings sponsored or co-sponsored by NASA.

- SPECIAL PUBLICATION. Scientific, technical, or historical information from NASA programs, projects, and missions, often concerned with subjects having substantial public interest.

- TECHNICAL TRANSLATION. English-language translations of foreign scientific and technical material pertinent to NASA's mission.

Specialized services that complement the STI Program Office's diverse offerings include creating custom thesauri, building customized databases, organizing and publishing research results ... even providing videos.

For more information about the NASA STI Program Office, see the following:

- Access the NASA STI Program Home Page at ***http://www.sti.nasa.gov***

- E-mail your question via the Internet to help@sti.nasa.gov

- Fax your question to the NASA STI Help Desk at (301) 621-0134

- Telephone the NASA STI Help Desk at (301) 621-0390

- Write to:
  NASA STI Help Desk
  NASA Center for AeroSpace Information
  7121 Standard Drive
  Hanover, MD 21076-1320

NASA/TM-2004-212991

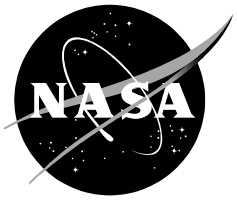

Wind Tunnel Application of a Pressure-Sensitive Paint Technique to a Faceted Missile Model at Subsonic and Transonic Speeds

Gary E. Erickson
Langley Research Center, Hampton, Virginia

National Aeronautics and
Space Administration

Langley Research Center
Hampton, Virginia 23681-2199

February 2004

Acknowledgments

The author would like to thank Dr. Blair B. McLachlan and Dr. James H. Bell of NASA Ames Research Center for their contributions that led to the establishment of a pressure-sensitive paint (PSP) system at the NASA Langley Research Center (NASA LaRC) 8-Foot Transonic Pressure Tunnel (8-Foot TPT). Their assistance in the definition, installation, and operation of the PSP system and the provision of the PAINTCP image processing software are greatly appreciated and respectfully acknowledged.

Special thanks are extended to Mr. Larry John and Mr. Clint Housh, Naval Air Warfare Center, China Lake, California, who were responsible for the design, fabrication, and testing of the missile model as part of a cooperative research program with NASA LaRC.

The author would also like to thank the PSP team headed by Mr. Clifford J. Obara at NASA LaRC, who provided technical assistance throughout the PSP testing at 8-Foot TPT. In particular, the contributions of Mr. Amir J. Jagharghi, Mr. B. Scott Sealey, Mr. Cecil G. Burkett, and Mr. Bradley D. Leighty are acknowledged with gratitude.

Special thanks are extended to the research and technical staff assigned to the 8-Foot TPT who supported the PSP testing in 1994 and, in particular, to Mr. Charles H. Fox and Mr. Sean M. Britton, who served as lead test engineer and lead technician, respectively. Their professionalism and support are appreciated and respectfully acknowledged.

Available from:

NASA Center for AeroSpace Information
7121 Standard Drive
Hanover, MD 21076-1320
301-621-0390

National Technical Information Service
5285 Port Royal Road
Springfield, VA 22161
703-605-6000

Abstract

A pressure-sensitive paint (PSP) technique was applied in a wind tunnel experiment in the NASA Langley Research Center 8-Foot Transonic Pressure Tunnel to quantify the vortex-induced surface static pressures on a slender, faceted missile model at subsonic and transonic speeds. Satisfactory global calibrations of the PSP were obtained at M_∞=0.70, 0.90, and 1.20, angles of attack from 10 degrees to 20 degrees, and angles of sideslip of 0 and –2.5 degrees using an in-situ method featuring the simultaneous acquisition of electronically-scanned pressures (ESP) at 57 discrete locations on the model. Both techniques clearly revealed the significant influence on the surface pressure distributions of the vortices shed from the sharp, chine-like leading edges. The mean error in the PSP measurements relative to the ESP data was approximately 0.6 percent at M_∞=0.70 and 2.6 percent at M_∞=0.90 and 1.20. The vortex surface pressure signatures obtained from the PSP and ESP techniques were correlated with the off-surface vortex cross-flow structures obtained using a laser vapor screen (LVS) flow visualization technique. The on-surface and off-surface techniques were complementary, since each provided details of the vortex-dominated flow that were not clear or apparent in the other.

Introduction

Global surface static pressure measurements are becoming more common in wind tunnel testing with the advent of the pressure-sensitive paint technique. A few of the pathfinding PSP applications for field measurements in aerodynamic testing are discussed in references 1 and 2. The key elements of a PSP system include a photoluminescent material in the form of a paint applied to the test article, an illumination source to excite the paint, an imaging device to document the paint in the excited state, and an image acquisition and processing system. A PSP system based on the work described in reference 2 was established in the NASA Langley Research Center (NASA LaRC) 8-Foot Transonic Pressure Tunnel (8-Foot TPT) in 1994. The practical application of this system to the measurement of the vortex-induced surface pressures on a slender, faceted missile model is discussed in this report. The global calibration of the PSP using discrete measurements from onboard ESP modules and the correlation of the surface measurements with qualitative off-surface flow visualization images obtained using a laser vapor screen technique are the focus of the discussion. The PSP system used in the 8-Foot TPT was subsequently transferred to the NASA LaRC Unitary Plan Wind Tunnel (UPWT) upon the closure of the former facility in 1995. Consequently, the description of the PSP system presented herein provides relevant historical material on the upgraded system currently in use at UPWT. Details of the UPWT PSP system are provided in reference 3.

Nomenclature

b reference span, 7.20 inches

$\bar{c}$ reference chord, 27.782 inches

C_p upper surface static pressure coefficient, $(p - p_\infty) / q_\infty$

$C_{p,v}$ vacuum pressure coefficient, $-2/\gamma M_\infty^2$

C_p^* pressure coefficient corresponding to the local speed of sound,

$$\frac{2}{\gamma M_\infty^2}\left\{\left[\frac{(\gamma-1)M_\infty^2+2}{\gamma+1}\right]^{3.5}-1\right\}$$

ESP	electronically-scanned pressure
ESP_i	pressure measurement at i^{th} orifice
LVS	laser vapor screen
M_∞	free-stream Mach number
N	number of ESP taps
p	local static pressure, pounds per square foot (psf)
p_0	stagnation pressure, psf
p_∞	free-stream static pressure, psf
PSP	pressure-sensitive paint
PSP_i	pressure measurement at PSP pixel location corresponding to i^{th} ESP calibration orifice
q_∞	free-stream dynamic pressure, psf
Re	Reynolds number per foot
s	local semispan measured from the body centerline to the leading (or trailing) edge, inches
S_{ref}	reference area, 1.2636 square feet
T_0	stagnation temperature, degrees Fahrenheit
M.S.	model station, inches
y	local semispan distance measured from the body centerline, positive to the right, inches
α	angle of attack, degrees
β	angle of sideslip, degrees
ε	mean relative error, percent

Model Description and Test Apparatus

The model used in this test was a 30 percent-scale model of a proposed missile concept. The model consisted of a slender lifting body with fixed tail. The body was faceted and featured chine-like cross sections with sharp leading edges. Figure 1 presents dimensional details of the missile model. Figure 2 is a photograph of the model installed in the test section of the 8-Foot TPT. A close-up view of the model is shown in figure 3. The model with PSP coating applied to the upper surface is illustrated in figure 4. There were six interchangeable noses which could be installed on the body. In addition, there were three interchangeable tail fins which could be installed on the body with either 45 degrees of anhedral or dihedral. The model also included a set of fin-off blocks. The PSP and ESP measurements presented in this report were obtained with a baseline nose and fins off. Figure 5 is a photograph of the model during pre-test assembly, which shows the noses, upper and lower body halves, and fin components and the balance and ESP instrumentation.

The model top and side views and cross-sections can generally be described as diamond shapes as previously shown in figure 1. The model had an expanding cross section forebody followed by a transitional region and, finally, a contracting cross section afterbody. The model leading and trailing edges were sharp-edge chines. The sharp leading edges were expected to develop leading-edge vortex flows. The flow field over the model was also expected to exhibit asymmetries at sufficiently high angles of attack because of the slenderness of the model and the development of multiple vortices arising from the discontinuities in the model planform and changes in the cross-sectional shape along the length of the model.

The ESP pressures were measured at selected stations by full rings of orifices. In terms of the local semispan, pressure orifices were placed at the body centerline (0 percent semispan) and in 5-percent increments to 95 percent semispan. The model length was 36 inches, and the pressure rings were placed at model station (M.S.) 9.0, 20.4, 25.5, 30.0, and 34.5 inches. This arrangement provided one ring on the forebody (M.S. 9.0), one ring in the transition region (M.S. 20.4), and three rings on the afterbody (M.S. 25.5, 30.0, and 34.5). The field-of-view that was selected for the PSP testing was the model upper surface and encompassed the pressure measurement stations at M.S. 20.4, 25.5 and 30.0. All of the PSP, ESP, and LVS results shown in this report correspond to these three model stations.

The model was instrumented with an internally-mounted, strain gauge balance to

measure the six force and moment components. Dedicated force and moment and ESP measurements were obtained on the unpainted model in separate phases of this test prior to the PSP testing. Balance and ESP measurements were also obtained during the PSP phase and were used, respectively, in the computations of the model attitude and global calibrations of the PSP. The balance chamber pressures were recorded, and the axial force was corrected to a condition of free-stream static pressure acting over the base area. Corrections for test section flow angularity were not applied, since previous testing of models of comparable size in this facility indicated these effects to be negligible. Blockage and wall interference corrections were not applied to the test data because of the relieving effect of the test section slots.

The model surface pressures were measured by four internally-mounted, 48-port ESP modules. These modules were 5 pounds per square inch differential (psid) pressure transducers which were referenced to the tunnel plenum pressure. Full on-line calibrations of the ESP transducers were performed at each change in the free-stream Mach number. The manufacturer-specified uncertainty in the pressure measurement as a percent of full-scale was +/-0.05 percent for the 5 psid modules. The mean relative error and the uncertainty in the PSP pressure measurements relative to the ESP data are presented in the Discussion of Results section.

Transition grit was applied according to the methods prescribed in reference 4. A transition ring consisting of #120 carborundum grains was applied to the nose in a 0.10-inch wide strip located 0.75 inches aft of the nose tip measured in a streamwise direction.

Wind Tunnel Facility and Test Conditions

The investigation was conducted in the NASA LaRC 8-Foot TPT. This wind tunnel facility was designed for operation as a continuous-flow, closed-return, variable-pressure wind tunnel with control capability to independently vary Mach number, stagnation pressure, stagnation temperature, and humidity. The test section was square with corner fillets and a cross-sectional area approximately equivalent to that of an 8-foot-diameter circle. The top and bottom walls of the test section were axially slotted to permit a continuous variation of the test section Mach number from 0.2 to 1.2; the slot-width contour provided a gradient-free test section 50 inches long for Mach numbers equal to or greater than 1, and 100 inches long from Mach numbers less than 1. The stagnation pressure could be varied from 0.25 to 2 atmospheres. Reference 5 provides a detailed description of the 8-Foot TPT. Note that this facility was permanently closed in 1995.

The PSP testing was performed at free-stream Mach numbers of 0.70, 0.90, and 1.20 at a Reynolds number of 3.0 million per foot and a stagnation temperature of 120 degrees Fahrenheit. The ESP measurements and the processed PSP images that are presented in this report were acquired at angles of attack from 12 degrees to 20 degrees in 2-degree increments at M_∞ = 0.70 and 0.90 and from 10 degrees to 20 degrees in 2-degree increments at M_∞ = 1.20. In addition, PSP images were acquired at α = 20 degrees and β = -2.5 degrees at M_∞ = 0.70, 0.90, and 1.20. The test conditions are summarized in Table I. The model angle of attack and angle of sideslip were determined via appropriate Euler angle transformations using the output from an accelerometer mounted in the base of the main sting support, output from a potentiometer installed in a yaw coupler mechanism, and angular deflection of the model, balance, and sting support system determined from pre-test calibrations.

M_∞	q_∞ (psf)	p_∞ (psf)	p_0 (psf)	Re (10^{-6})	T_0 (^0F)
0.70	448	1304	1812	3.0	120
0.90	536	942	1598	3.0	120
1.20	625	618	1504	3.0	120

Table I. Test conditions for the faceted missile model experiment.

The LVS flow visualization was performed in a separate phase of the experiment at M_∞ = 0.90 and 1.20. The LVS cross-flow images presented in this report coincide with the model pressure measurement stations and angles of attack at which the PSP and ESP measurements were obtained. LVS flow visualization was not possible at M_∞ = 0.70, since the estimated amount of water injection to promote local condensation of water vapor in the test section was prohibitive. Flow visualization images at β = -2.5 degrees were obtained only at M_∞ = 0.90.

Experimental Techniques

Pressure-Sensitive Paint Technique

The PSP method is based on the oxygen-quenching characteristics of certain luminescent materials. The emitted light intensity varies inversely with the local oxygen partial pressure and, therefore, the air pressure, since oxygen is a fixed mole fraction of air. A PSP formulation typically consists of three components. The luminescent material (luminophore) is the sensor component. For oxygen quenching to occur, the luminophore must be soluble in a suitable binder material. Finally, a compatible solvent is used for the application of the paint, via a spray gun, to the test article. Prior to the paint application, the model surface is primed with white paint. The white undercoat to the PSP coating serves a critical function in that it amplifies the PSP emission signal (reference 2). Certain characteristics of PSP coatings induce measurement error: photodegradation and temperature sensitivity. Specifically, the emission response of the PSP decreases with time of exposure to the excitation radiation, and the luminescence intensity is sensitive to changes in the temperature. An earlier formulation successfully applied at the 8-Foot TPT was designated IEMA/PtT(PFP)P, which used a proprietary University of Washington copolymer (IEMA). Laboratory calibrations at LaRC indicated that the Stern-Volmer characteristics (reference 2) were very linear, and photodegradation was reduced compared to prior-generation paints. This formulation was not the most advanced in current use by other facilities; however, it proved a robust and responsive formulation for use at the low static pressures typical of the transonic testing at the 8-Foot TPT.

The intensity of the light emitted by the PSP is proportional to the excitation light that is absorbed. A stable illumination source must be used that is tailored to the absorption wavelength band of the PSP coating. Ultraviolet long wave (365 nm), 250-watt lamps connected to a regulated power supply were used in continuous mode to provide the illumination source in the 8-Foot TPT system. The optical filters attached to these lamps allowed passage of light at the absorption wavelength of the coating but prevented transmission of light at the luminescence wavelengths that could compromise the images acquired by the PSP camera. Figure 6 presents a simplified sketch of the main components of the 8-Foot TPT PSP system.

Electronic CCD imaging devices of two types were used: conventional video and scientific grade digital cameras. The original PSP system used at the 8-Foot TPT featured an 8-bit resolution image acquisition and processing system using standard NTSC format video cameras. These cameras continued to be used in an upgraded PSP system as monitoring devices only, since they had the advantage of providing real-time viewing of the PSP response to aerodynamic flow changes. A scientific-grade, thermoelectrically-cooled digital camera connected to a regulated power source was used for PSP image acquisition because of its low noise, excellent linear response, and good signal-to-noise ratio. This camera acquired an electronic snapshot only, and the exposure or integration time was set from the host computer. The experiment described in this report was the first application of the 8-Foot TPT PSP system using a cooled CCD digital camera of 14-bit resolution and 1024 x 1024 pixel array. This camera could be commanded to acquire an image with the lens closed in order to acquire a

"dark image". A dark-level correction was applied to all wind-off and wind-on images to subtract out the CCD dark current and "noise" of the overall imaging system. Optical filters centered about 650 nm were installed on the conventional video and scientific-grade digital cameras to permit the passage of the luminescence emission wavelengths, while preventing the transmission of the excitation light source wavelengths to the acquisition cameras. The incursion of extraneous sources of light from the plenum area into the test section was prevented by turning off all light sources within the plenum and sealing all optical view ports into the plenum with "light-tight" coverings.

Acquisition of the PSP images was controlled by a personal computer (PC)-based workstation in the 8-Foot TPT control room. The cable run length between the host computer and the camera installed above the test section was approximately 100 feet. The digital camera and its electronic control and liquid cooling units were connected to a proprietary image acquisition board installed in the PC via a custom electronics cable. The proprietary image acquisition software on the PC provided a full-featured suite of utilities to evaluate the characteristics of an acquired image. However, the time-critical nature associated with the acquisition of images during the testing typically precluded the use of anything but the most basic features. Images were stored on high-capacity optical disks for off-line processing and archiving. Image processing was performed on a high-end workstation using the software package described in reference 6 and referred to as PAINTCP.

Optical access to the 8-Foot TPT test section was provided by several schlieren windows on both sidewalls and three identical 4-inch wide by 16-inch long optical-quality windows positioned along the centerline of the test section ceiling. The imaging cameras and ultraviolet light sources were installed in the test section ceiling in order to image the upper surface of the missile model at high angles of attack. Special pressure- and thermally-controlled enclosures were used to protect the imaging cameras, which were exposed to the low-pressure environment within the plenum. Temperature control within the enclosures was achieved by vortex-tube coolers attached to each unit. Coolers were also installed to the four UV lamp heads to avoid temperature-induced damage to the electronic circuitry that occurred in previous PSP testing at 8-Foot TPT and in similar pressure tunnels. In addition, vortex coolers were used to provide cooling air along the optical windows to avoid thermal stresses induced by the UV lamps, which were in proximity to the window surface. A total of four 250-watt UV lamps were installed along the ceiling centerline, two in front of and two behind the imaging cameras. Metal shields were placed between the digital camera and lamps to prevent electromagnetic interference that could damage the camera's sensitive electronic components, which might occur as the result of power cycling of the UV lamps while the camera was operational. Previous testing experience at the 8-Foot TPT indicated the vibration level within the ceiling region was sufficiently low that preventative measures for safe operation of the digital camera were unnecessary. The imaging and illumination devices were attached to regulated power sources, which could be independently controlled (on/off) from the wind tunnel control room. The complexity of the hardware installation on top of the wind tunnel test section is revealed in the photographs in figure 7.

The paint application and curing process required one working shift to complete. This operation required a skilled painter equipped with protective gear, including full face mask and a continuous air supply. The missile model was instrumented with discrete surface static pressure orifices plumbed to internal, 5 psid ESP modules. Modules with purge air capability were not available at the time of this experiment. Consequently, the pressure rows were masked off with 0.06-inch wide tape during the painting process. An alternate approach was used on one pressure row, where the orifices were individually sealed with small cotton swabs in

an attempt to obtain usable painted area between the orifices. This approach met with only marginal success. Approximately 4 hours were required for the curing of the base coat, and a comparable period of time was allotted after the PSP coating was applied. The PSP image registration process required that reference marks, or control points, be placed on the model. The locations of these registration marks were defined by placing on the fully-cured PSP coating a Mylar transfer sheet containing a 1:1 scale drawing of the missile model with pre-punched holes. After the hole centers were marked, the Mylar template was removed and black dots were drawn on the model using a plastic circle template and a black marker pen. Latex gloves were worn during this process to avoid contamination of the PSP coating.

Wind-off images were acquired at several angles of attack with the test section pumped down to a low pressure of approximately 300 psf. This condition was more representative of the static pressure levels that existed on the painted model during wind-on runs, and it provided an opportunity to define a digital camera integration time that would be used throughout the testing. In general, a range of integration time was determined from the wind-off run such that the maximum pixel intensity was approximately 60-70 percent of the saturation level of the camera. This approach provided a buffer against saturation during the wind-on runs where lower static pressures that occurred locally on portions of the model promoted even higher pixel intensities at the same integration times. Integration times of 500 milliseconds (msec) to 1500 msec were typical. The longer integration times were a potential issue in the event of model vibration during the acquisition of the PSP images.

Wind-on data acquisition consisted of the discrete pressures measured from the ESP taps and the PSP images at the desired angles of attack. Full on-line calibrations of the ESP modules were performed at each change in the Mach number, since the acquisition of high-quality ESP data was essential to the in-situ PSP calibrations performed during the off-line image processing. The PSP illumination sources could not be shielded during the transitional phases of tunnel operation such as Mach number and angle of attack changes and ESP calibrations. Consequently, run times were kept to a minimum in order to limit the overall exposure time of the PSP coating. PSP image acquisition was performed independently of the data acquisition performed by the wind tunnel host computer. The test conditions, ESP data, and other parameters were obtained off-line for use in input files required by the PSP image processing software. A repeat set of wind-off images and dark images were acquired after the wind-on runs. Comparisons of the initial and final wind-off pixel intensities at the same camera integration times provided an indication of the level of photodegradation that had occurred.

The image processing method featured the subtraction of the dark image from the wind-off and wind-on images, identification of wind-off and wind-on control points, image registration, image ratioing, resection transform, and global calibration of the paint. Registration, or spatial alignment, of the two model images was performed to correct for nonalignment caused by model motion. A second-order biquadratic transform was used to align the wind-on image with the wind-off image. This process depended on finding the respective control points, or registration marks, which were used to determine the transform coefficients. The wind-off and wind-on intensity field images were ratioed, and the intensity field of the resultant image was proportional to pressure (Stern-Volmer relation). A resection transform based on photogrammetry techniques was performed next, which related each point in the final intensity ratio image plane to a corresponding point on the model surface. The effectiveness of this transform depended on an accurate determination of the spatial locations of the model registration marks. The image mapping performed in this experiment was exclusively a 2-D plane view representation of the missile model. Quantification of the pressure field in

the final intensity ratio image required a calibration of the paint to determine the Stern-Volmer sensitivity coefficients. An "in situ" calibration method was applied, where the paint intensity was calibrated from the pressure tap data at spatially corresponding locations. The in-situ calibration process was iterative, since the first pass through the calibration rarely provided a completely satisfactory global match between the ESP and PSP pressure data. Because of the masking approach that was used during the paint process, the paint could not be calibrated at the exact locations of the pressure orifices. This required that the PSP image pixel locations used for calibration be offset from the orifice. In some instances, apparent nonuniformity of the paint thickness near the masking lines required additional offsets during the calibration procedure.

Laser Vapor Screen Technique

The vapor screen method of flow visualization has been used in wind tunnel testing for several decades to visualize vortices, vortex sheets, lines of flow separation and reattachment, and shock waves at subsonic, transonic, and supersonic speeds. Water is injected in sufficient quantity into the tunnel circuit, typically downstream of the supersonic nozzle or the diffuser section, to cause condensation of water vapor in the test section. At supersonic speeds, the temperature drop from the expansion in the supersonic nozzle causes the water vapor to condense into a fine fog. A laser is often used to produce an intense sheet of light that is projected into the test section in a plane perpendicular to the longitudinal axis of the tunnel or to the body axis of the model. The distribution of condensed water vapor and, consequently, the amount of scattered light within the plane of the light sheet is affected by the flow disturbances created by the model. This phenomenon permits the observation and documentation of vortex cross sections, for example, at high angles of attack. Condensation first appears in the free stream at supersonic speeds, so the vortical flows appear as dark regions in the absence of scattered light surrounded by a light background. At subsonic and transonic speeds, condensed water vapor generally first appears near the central region of the vortices, so the vortex cross sections appear as light regions within a darker background. A combination of the two light-scattering patterns often occurs at transonic speeds.

A fiber-optic-based laser vapor screen (LVS) system was established in the 8-Foot TPT in 1990 (reference 7) to visualize the vortex-dominated flow fields about small-scale models of fighter aircraft, commercial transport airplanes, and missiles at subsonic and transonic speeds. A simplified sketch of the 8-Foot TPT system is shown in figure 8, and a detailed description of this system is provided in reference 7. A fiber optic cable delivered a beam from an argon laser located outside the tunnel plenum to a light sheet optics package located in the ceiling of the test section. The optics package occupied the same region required by the PSP hardware, so the setup of the two techniques was mutually exclusive in this facility. Consequently, application of the two techniques was performed in separate phases of the experiment. The fiber-optic-based beam delivery system contained five principal components: laser-to-fiber coupler, armored fiber optic cable, remote light sheet generator, rotating mirror, and optics motor controller. The system was designed to be used with virtually any argon-ion laser system operating in either continuous wave (CW) or multimode with beam diameters from approximately 0.0315 inches to 0.0709 inches. The light sheet optics package allowed variation of the sheet thickness, divergence or spread of the light sheet, and sheet rotation relative to the model. A 3- by 3-inch mirror mounted onto a rotational stage with 360 degrees of continuous rotation directed the light sheet through the optical window and to the desired station on the model. The light sheet was aligned to be perpendicular to the model surface at mid body length and an angle of attack of 16 degrees. Because the light sheet swept in an arc along the model, it was nonorthogonal with respect to the model surface at all other conditions.

Water was injected into the tunnel circuit from a 150-gallon tank of deionized water located in a room on top of the plenum shell to an array of six atomizer nozzles installed in the ceiling region of the diffuser section. The amount of water that was injected into the tunnel was remotely regulated from the wind tunnel control room via a solenoid switch and a one-horsepower pump positioned on the discharge side of the water tank.

Documentation of the LVS images was obtained using a miniature video camera with 360 television lines of horizontal resolution and a fixed focal length lens contained in a cylindrical housing mounted onto the model sting support system. This camera provided a perspective aft of the model which looked upstream along the model centerline. The video image perspective remained constant throughout the pitch angle range because there was no relative motion between the camera and the model. The video image perspective did vary, however, if the model yaw angle was changed. Selected portions of the videotape recording were digitized and converted to AVI format using a video frame grabber installed in a personal computer. The frame grabber software allowed the precise capture and enhancement of the individual LVS frames that appear in this report.

Discussion of Results

PSP Benefits and Accuracy

The PSP pressure measurement technique allowed for a more detailed view of the vortex-induced pressure field on the missile model upper surface compared to the three rows of ESP taps that are highlighted in this report. An advantage of the PSP technique is that every pixel in the painted portion of the image is effectively a pressure tap, so the pressure distributions can be resolved to much greater detail in all applicable regions of the model.

Table II summarizes the percent error in PSP pressure measurement relative to the ESP tap data for the selected conditions of M_∞ = 0.70, 0.90, and 1.20, α = 20 degrees, and β = 0 degrees. Listed in this table are the Mach number, the number of ESP taps used to calibrate the PSP, the range of pressure spanned by the ESP taps, the mean relative error in PSP measurement, and a 95 percent confidence interval (C. I.) in the PSP measurement.

M_∞	N	Range of ESP pressures (psi)	$\varepsilon(\%)$	95% $C.I.$ for $ESP_i - PSP_i$ (psi)
0.70	57	6.6 - 8.7	0.6	+/-0.12
0.90	57	6.7 - 8.7	2.6	+/-0.33
1.20	56	2.1 - 3.4	2.6	+/-0.22

Table II. Summary of PSP analysis results for three wind tunnel conditions.

The mean relative error is calculated using the following equation from reference 8:

$$\varepsilon = \frac{\sum_{i-1}^{N}\left(100 \times \frac{\left|ESP_i - PSP_i\right|}{ESP_i}\right)}{N}$$

where ESP_i is the pressure value at the i^{th} pressure tap, PSP_i is the pressure value using the PSP technique corresponding to ESP_i, N is the number of ESP taps used , and ε is the mean relative error in pressure measurement using the PSP technique. This table indicates that the mean relative error in pressure measurement is larger at the transonic Mach numbers compared to the subsonic Mach number. The uncertainty in the PSP measurement is also higher at the transonic speeds. It is not possible to attribute this trend to any specific source. However, possible contributing factors are (1) error in the intensity measurement, which results in a larger relative error in the measurement of low pressures compared to high pressures (reference 9); (2) increased model vibration at the transonic speeds, particularly at the M_∞ = 0.90 condition; (3) more pronounced surface temperature variations at the transonic speeds (surface temperature measurements were not made during this experiment); (4) photodegradation

effects (the transonic images were acquired at a later time in the run sequence compared to the subsonic images); (5) the presence of local condensation (humidity control was used in the 8-Foot TPT but instrumentation to measure humidity was not available). It is noted, however, that the magnitudes of the relative error and uncertainty levels are encouraging, given the developmental status of the 8-Foot TPT PSP system at the time of this experiment.

PSP and ESP Pressure Measurements and LVS Flow Visualization

Composite plots are presented in the following sections showing the distributions of the calibrated PSP upper surface static pressure coefficient corresponding to the locations of the discrete ESP pressure orifices at M.S. 20.4, 25.5, and 30.0. The surface pressures are plotted against the local distance *y* measured from the body centerline, normalized by the local semispan, *s*. For example, values of the nondimensional semispan location *y/s* = -1.0, 0.0, and 1.0 correspond to the left leading edge (or trailing edge, depending on the measurement station), body centerline, and right leading edge (or trailing edge), respectively.

There were 19 discrete pressure orifices on the upper surface within each measurement station. Occasionally, measurements at a limited number of orifice locations were considered questionable based on the pressure coefficient levels relative to adjacent orifices. These possible outlying measurements were influential in the global calibration of the PSP. A review of the transducer output and the reasonableness of the pressure coefficients in the context of the observed vortex flow behavior provided a screening mechanism for potential outlying/influential observations.

A global calibration of the PSP was obtained by selecting pixel locations in the processed PSP image that were as close as possible to the ESP pressure orifices but in a region where the paint thickness was considered uniform. There was an unpainted region about 0.06 inches wide centered about the pressure orifices. In addition, there was a transition region where the PSP was feathered into the unpainted area. A typical pixel location for calibration purposes was approximately 0.05 inches from the orifice.

All plots contain a false-colored PSP image which has undergone registration, ratioing, resection transform, and calibration, as noted by the color-coded pressure coefficient bar adjacent to each PSP image. Where available, LVS images obtained at each pressure measurement station are shown above the corresponding PSP and ESP pressure distributions. The main purpose of these composite plots is to show the level of agreement between the two pressure measurement techniques and to provide pertinent information on the topology of the vortex flows that induce these pressure distributions.

$M_\infty = 0.70$

Comparisons of the distributions of the PSP and ESP upper surface static pressure coefficient at M_∞ = 0.70 and α = 12, 14, 16, 18, and 20 degrees and β = 0 degrees are shown in figures 9(a) through 9(e), respectively. Figure 9(f) compares the corresponding surface pressures at α = 20 degrees and β = -2.5 degrees (model nose oriented to the right of the free stream direction). The false-colored PSP images and the associated color bars reveal the surface pressure field response, where regions of higher suction pressures (more negative pressure coefficients) are denoted by light-to-dark green and light-to-dark blue colors. Regions of lower suction pressures (less negative pressure coefficient) or small positive pressures are represented primarily by yellow, orange, red, and lavender colors. The range of pressure coefficient denoted in the color bars is generally different at each angle of attack. This range was specified within the PSP image processing software to reveal the best possible details of the vortex-induced pressure signature. Specification of a common pressure coefficient range for all angles of attack

would have resulted in relatively large uninterpretable white or black regions in certain images. In general, the pressure signature, or footprint, of the leading-edge vortex along the forebody and the transitional region of the body is revealed by a narrow band of light-to-dark blue colors that is bounded on its outboard edge by dark green colors and on the inboard edge primarily by various shades of green and yellow. The vortex footprint is less pronounced, but still discernible, along the afterbody and is typically represented by a wider band of green bounded by yellow and red colors.

The PSP and ESP pressure distributions are in reasonable agreement at α = 12 degrees (figure 9(a)). Both pressure measurement techniques reveal distinct leading-edge vortex-induced suction pressure peaks centered at approximately 62.5 percent of the local semispan at all three measurement stations. The vortical flow pressure signature is nonconical. This is due to the upstream influence of the trailing-edge pressure recovery that causes the vortex-induced suction pressure peak to diminish from the forward to aft measurement stations at a given angle of attack. The transition in the PSP image from a narrow band of dark blue colors along the forebody to a broader region of dark green, light green, and yellow colors on the afterbody is consistent with the diminished vortex pressure signature and a broadening of the vortical flow along the length of the missile model.

Good agreement between the PSP and ESP pressure distributions is also apparent at α = 14 degrees to 20 degrees (figures 9(b) – 9(e)). Both techniques effectively capture an increase in the vortex-induced suction peaks and a slight inboard movement of the vortex pressure signature at a given pressure measurement station caused by increasing the angle of attack. The pressure distributions suggest that the leading-edge vortex is stable up to at least 20 degrees angle of attack, which is an expected result given the slenderness of the missile model. The occurrence of vortex breakdown would be manifested by a flattening of the spanwise pressure distribution, decreased suction pressure levels, and a loss of the vortex pressure signature in the PSP image. Note that the peak suction pressure coefficients obtained at M.S. 20.40 and α = 20 degrees marginally exceed the value of the critical pressure coefficient, C_p^* = –0.779, at M_∞ = 0.70. This indicates that locally supersonic flow occurs near the surface of the missile body underneath the leading-edge vortices at this measurement station.

Beginning at about α = 16 degrees (figure 9(c)), a second, less pronounced suction pressure peak located outboard of the primary peak occurs in the PSP and ESP distributions at M.S. 20.40. This second peak might be interpreted as the signature of a secondary vortex (reference 10). It will be shown in the LVS images in the next section, however, that this second peak is likely induced by another primary leading-edge vortex. A phenomenon referred to as "vortex sheet tearing" may occur, where the leading-edge vortex that is shed from the forebody tears away from the leading edge along the transition section of the body. This allows the formation of a second, smaller vortex along the remaining length of the leading edge. The presence of this second vortex does not persist at M.S. 25.50 and M.S. 30.00 because it is entrained into the more dominant forebody vortex.

The afterbody portion of the PSP images and the PSP pressure distributions at M.S. 30.00 are not entirely symmetric with respect to the model centerline. This asymmetry is more apparent at the higher angles of attack, for example, at α = 18 degrees and α = 20 degrees in figures 9(d) and 9(e), respectively. In contrast, asymmetry is not apparent in the ESP distributions at M.S. 30.00. This was a persistent trend in the current experiment and was more pronounced in subsequent runs at the higher Mach numbers. A definitive explanation for this discrepancy is not available at this time. Nonuniformity of the paint thickness on the missile upper surface is a possible contributing factor. In addition, the placement of the UV lamps in the test section ceiling and/or nonuniformity of the UV lamp output are factors that might cause nonuniform

PSP photodegradation and a resultant pseudo asymmetry in the calibrated surface pressures.

The PSP and ESP pressure distributions clearly reveal the effect of sideslip on the upper surface static pressure distributions in figure 9(f) at α = 20 degrees and β = -2.5 degrees. The pressure distributions are very asymmetric at all three measurement stations. More pronounced vortex-induced suction pressure peaks are observed on the windward side (in this case, the left-hand side of the missile) compared to the leeward (right-hand) side. A similar effect of sideslip on forebody vortex-induced pressure distributions was documented in reference 11. The LVS images presented in the next section at M_∞ = 0.90 provide a qualitative explanation for this effect. The false-colored PSP image reveals a narrow blue band of high suction pressures underneath the windward vortical flow. A similar pressure footprint is absent on the leeward side. The quantitative agreement between the PSP and ESP pressure measurements is satisfactory at M.S. 20.40 and 25.50. Supercritical flow occurs under the windward vortex at M.S. 20.40, since the suction pressure peak exceeds the critical pressure coefficient of –0.779. The windward vortex pressure signatures are in good agreement at M.S. 30.00, but the suction pressure levels induced by the leeward vortex are noticeably higher in the PSP measurements compared to the ESP tap data. Examination of the leeward vortex pressure signatures at M.S. 20.40 and 25.50 and consideration of the nonconical flow behavior suggests that the ESP data are a better representation of the pressure distribution in this region.

M_∞ = 0.90

Figures 10(a) through 10(e) compare the PSP and ESP pressure measurements at M_∞ = 0.90, α = 12, 14, 16, 18, and 20 degrees, and β = 0 degrees, respectively. LVS images are also displayed above the pressure distributions at each measurement station. A similar composite plot is presented in figure 10(f) corresponding to α = 20 degrees and β = -2.5 degrees.

The PSP and ESP pressure measurements exhibit favorable agreement at α = 12 degrees in figure 10(a). The nonconical vortical flow pressure signature is apparent, where the magnitudes of the vortex suction peaks and the overall suction pressure levels induced by the vortex diminish from the forward to the aft measurement stations. The processed PSP image reveals a narrow region of higher suction pressures along the missile body that define the vortex pressure footprint. The PSP surface signature is consistent with the off-surface LVS images, which show a small, concentrated vortex in proximity to the missile body. The model was painted flat black for the LVS flow visualization and was contrasted with a relatively dark background. Consequently, details of the model are difficult to discern in these images. However, the left and right leading (or trailing) edges at each light sheet location are established by the outer edges of the light sheet projected onto the model surface. It is noted that the LVS images in figure 10(a) do not reveal the entire topology of the leading-edge vortices. All that is revealed is a small region near the center of the vortices where the water vapor has condensed, given the conditions in the wind tunnel at that time. More details might have been revealed at this angle of attack by injecting additional water into the tunnel circuit and by reducing the stagnation temperature below 120 degrees Fahrenheit. However, increased water injection would likely have yielded too much condensation and, consequently, compromised the clarity of the images at the higher angles of attack. Maintaining a lower stagnation temperature was an elusive goal given the high outside summer temperatures that existed at the time of this experiment.

Comparison of the PSP and ESP pressure coefficients in figure 10(a) to the critical value of –0.188 at M_∞ = 0.90 indicates that the flow is entirely supersonic at M.S. 20.40. At M.S. 25.50, a supercritical region exists under the vortical flows. The flow is subcritical at M.S. 30.00.

The PSP and ESP surface pressure distributions at α = 14 to 20 degrees in figures 10(b) through 10(e) exhibit reasonable agreement. Both techniques effectively capture the increase in the magnitudes of the peak suction pressure coefficients and an inboard movement of the vortex pressure footprint at each measurement station caused by increasing the angle of attack. The increase in the suction peak magnitude, which is an indicator of the vortex strength, is more modest compared to the results obtained at M_∞ = 0.70. This is an expected trend with increasing Mach number (references 10 and 12). An interesting feature of the processed PSP images at these angles of attack are striation patterns underneath the vortical flows along the afterbody region. This phenomenon is attributed to the structure of the leading-edge vortex, which is not composed of a continuous feeding sheet from the leading edge but, instead, of numerous vortices arising from shear layer instabilities along the length of the leading edge. These shear layer instabilities have been observed in many wind tunnel flow visualization experiments and in natural condensation patters of aircraft in flight. A detailed summary of these observations is presented in reference 13. Another feature of the PSP images at these angles of attack is the absence of red-coded pressure coefficients about the body centerline in the transition region. It is speculated that a flow expansion occurs along the upper surface in the transition region followed by a pressure recovery and the appearance of red-coded pressures along the afterbody. The inboard movement of the vortex-induced reattachment position along the aft region of the body may also contribute to the pressure rise along the body centerline. The images presented in figures 10(b) – 10(e) are illustrative of some of the more subtle details that may be present in the PSP surface pressure response.

The region on the missile upper surface where the measured static pressure coefficient exceeds the critical value of –0.188 broadens as the angle of attack increases. The PSP and ESP pressure distributions are entirely supercritical at M.S. 20.40 and at all angles of attack. Large pockets of supersonic flow underneath the vortices are inferred from the pressure distributions at M.S. 25.50 and 30.00, although the spanwise extent at a given angle of attack depends on the pressure measurement technique. The differences are most pronounced at the aft measurement station, where the PSP distribution and processed image reveal asymmetries in the spanwise distribution of the pressure coefficient and the color-coded surface pressure response. The ESP distributions at M.S. 30.00 are reasonably symmetric, and the LVS images do not reveal any obvious asymmetries in the off-surface flow field.

The LVS flow visualization images in figures 10(a) – 10(e) illustrate the growth of the leading-edge vortices at a given pressure measurement station that is caused by increased angle of attack. This provides a qualitative, off-surface perspective that is consistent with the higher suction pressure levels (stronger vortices) exhibited in the PSP and ESP measurements. The vortex cross sections at M.S. 20.40 and 25.50 are approximately circular. The more unusual vortex cross section at M.S. 30.00 at all angles of attack is indicative of the interaction of two, co-rotating vortices. The vapor screen image at M.S. 25.50 and α = 16 degrees (figure 10(c)) suggests the existence of a leading vortex feeding sheet discontinuity, where the vortex generated along the forebody region tears away from the leading edge, thereby allowing the development of a second, smaller vortex rotating in the same sense from the transition region of the body. The latter vortex is entrained into the dominant forebody vortex, and it appears as a spiral discontinuity at the outer edge of the vortex cross flow images at M.S. 30.00 and at all angles of attack. The existence of the second vortex is, perhaps, most clearly shown in the images at M.S. 25.50 and α = 18 and 20 degrees in figures 10(d) and 10(e). The pressure signature of this vortex may be inferred from the PSP and ESP pressure distributions as a second, less pronounced suction peak outboard of the primary peak at M.S. 20.40 and angles of attack from 14 degrees to 20 degrees in figures 10(b) – 10(e). A similar effect was noted in the previous section at M_∞ = 0.70. The signature of the

second vortex is no longer apparent at M.S. 25.50 and 30.00 because of its interaction with the stronger forebody vortex. The processed PSP images also provide some hint of the existence of a multiple vortex system, since there is a small region of high suction pressures (blue color) situated along the transition region of the body and outboard of the primary vortex pressure signature.

The nonconical nature of the leading-edge vortex pressure signature that was cited at M_∞ = 0.70 in the previous section is also observed at M_∞ = 0.90. The decrease in the overall vortex-induced suction pressure levels at a given angle of attack may be more abrupt from M.S. 20.40 to M.S. 25.50 because of the discontinuity in the leading-edge sweep angle. The body chine is essentially a trailing edge downstream of the planform break, and it is presumed that vorticity is no longer feeding into the vortex from this point aft. Consequently, the flow about the afterbody section is characterized by a "free" vortex system. This hypothesis is supported by the LVS images. At α = 18 and 20 degrees (figures 10(d) and 10(e)), for example, the condensation patterns at M.S. 20.40 indicate that the vortex is attached to the leading edge by a "feeding sheet." At M.S. 30.00, however, a band of condensation connecting the vortex to the edge of the body is not apparent, which suggests that a free vortex traverses this region of the model. The vortex does appear to be larger at M.S. 30.00 compared to the pattern at M.S. 25.50. This qualitative result implies vortex growth and, hence, a vorticity-feeding mechanism. However, the streamwise accumulation of water vapor condensate and the interaction of two, co-rotating vortices may yield an illusion of a larger vortex along the afterbody. The lack of a connecting leading-edge feeding sheet is considered more powerful evidence of a free vortex system.

Figure 10(f) presents a composite plot at α = 20 degrees and β = -2.5 degrees. The spanwise distributions of the PSP and ESP static pressure coefficient are asymmetric at M.S. 20.40, 25.50, and 30.00, and the most pronounced vortex-induced suction peaks occur on the windward side of the body. The PSP and ESP pressure measurements agree very well at M.S. 20.40 and 25.50, and both techniques capture the pressure signatures of the windward and leeward vortices. The higher PSP suction pressures near the leeward leading edge at M.S. 20.40 are attributed to a deficiency in the global calibration of the paint in this region and not to a real flow phenomenon. The PSP and ESP measurements are in quantitative agreement on the windward side at M.S. 30.00, but the PSP measurements show significantly higher suction pressure levels on the windward side compared to the ESP tap data. This is also considered a shortcoming in the paint calibration, and may be caused by nonuniformities in the paint thickness, UV illumination, and/or photodegradation as cited in the previous section corresponding to M_∞ = 0.70. Comparison of the measured pressure coefficients to the critical value, C_p^* = –0.188, indicates that the PSP and ESP distributions at M.S. 20.40 are supercritical at all PSP pixel/ESP tap locations. The flow is entirely supersonic underneath the windward vortex at M.S. 25.50 and 30.00, and a pocket of supercritical flow exists under the leeward vortex at M.S. 25.50. The large discrepancies between the PSP and ESP measurements on the leeward side at M.S. 30.00 lead to different inferences regarding the existence of supercritical flow in this region. The ESP tap data suggest the flow is subcritical, whereas the PSP measurements imply a large pocket of locally supercritical flow. The ESP measurements are considered more consistent with the overall data trends at this high angle-of-attack, sideslip condition. The processed PSP image reveals a pressure signature of the windward vortex, which is discernible as a narrow band of blue and dark green colors over most of the exposed model length. In addition, there is another region of high suction pressures on the windward side along the transition region of the body. In contrast, the pressure signature of the leeward vortex is barely visible along the forebody region, and it cannot be detected along the afterbody. Good qualitative correlation exists between the PSP image, the PSP and ESP pressure measurements, and the LVS images. At M.S. 20.40, the windward vortex is close to the

missile upper surface and is attached to the leading edge by a band of condensate. The leeward vortex is situated farther above the surface, and there is no evidence of a feeding sheet connecting the vortex to the leading edge at this measurement station. In sideslip, the windward vortex moves closer to the model surface while the leeward vortex migrates away from the surface. This effect contributes to the higher PSP and ESP suction pressure levels compared to the leeward side. In addition, the effective decrease in the leading-edge sweep on the windward side yields a stronger vortex at a given angle of attack, whereas the opposite effect occurs on the leeward side (reference 14). Similar trends are observed at M.S. 25.50 and 30.00. The development of a second, co-rotating vortex is apparent at M.S. 25.50 along the transition region of the body on the windward side. This smaller, weaker vortex is observed to orbit about the dominant forebody vortex at M.S. 30.00, which remains in proximity to the model surface. As a result, a highly peaked windward pressure distribution is still observed in the PSP and ESP measurements at this model station. By comparison, the apparent free vortex system on the leeward side induces more subtle PSP and ESP suction pressure levels, which are significantly less in magnitude than the corresponding levels on the windward side.

M_∞ = *1.20*

Figures 11(a) through 11(f) compare the PSP and ESP pressure measurements at M_∞ = 1.20, α = 10, 12, 14, 16, 18, and 20 degrees, and β = 0 degrees, respectively. Note that this is the only Mach number at which PSP and ESP pressure measurements and LVS flow visualization were obtained at α = 10 degrees. The LVS images are displayed above the pressure distributions at each measurement station. A comparison plot of the PSP and ESP pressure measurements is presented in figure 11(g) corresponding to α = 20 degrees and β = -2.5 degrees . LVS images were not obtained at this test condition.

The global calibration of the PSP using the ESP tap data at α = 10 degrees (figure 11(a)) was generally satisfactory, except at M.S. 30.00 where the PSP suction pressure levels are significantly higher over most of the starboard side of the body. This discrepancy is common to the results obtained at all Mach numbers in this experiment. At all other locations, the PSP and ESP measurements are in quantitative agreement, and both methods reveal the suction pressure signatures associated with this vortex-dominated flow field. Dual suction peaks are observed on either side of the model centerline at M.S. 20.40. This pressure distribution is assumed to be induced by the dual co-rotating vortex system previously discussed in the sections corresponding to M_∞ = 0.70 and 0.90. The second, smaller vortex is not visible in the LVS image at this measurement station, since is hidden by the sloping surface of the model. A frame-by-frame review of the original LVS flow visualization recording does show a small vortex near the leading edge a short distance downstream of M.S. 20.40. Interestingly, this second vortical flow is more clearly seen in the LVS image at M.S. 25.50, but its pressure signature is absent. This effect arises from the displacement caused by an interaction with the primary forebody leading-edge vortex. The nondimensional semispan location of the primary vortex-induced suction peaks moves outboard from M.S. 20.40 to M.S. 30.00, which is opposite to the trend observed in the results presented at M_∞ = 0.70 and 0.90. This effect is caused by the interaction of the two co-rotating vortices, which is apparent in the LVS image at M.S. 30.00. A small, circular region void of condensate in the cross-flow pattern on either side of the model centerline is actually the core of the second vortex that is shed from the transition region of the body. At higher angles of attack where the primary forebody vortex dominates the flow field, the vortex suction peaks typically move outboard from the forward to aft regions of the model. The vortex footprint in the processed PSP image is marginally discernible. Although the vortices are prominent features of the off-surface LVS images, they are relatively weak at this moderate angle of attack and higher Mach number. Consequently, the surface pressure response in the PSP image is more subtle.

The PSP response in the processed images is more definitive at the higher angles of attack in figures 11(b) – 11(f), where the narrow band of blue and dark green colors reflect the stronger vortical flows. The agreement between the PSP and ESP measurement techniques is generally very good at M.S. 20.40 and 25.50 at all angles of attack, whereas the agreement is less satisfactory at M.S. 30.00. The PSP and ESP pressure distributions are more conical in nature over a portion of the model length compared to the trends observed at the lower Mach numbers. For example, the footprints of the vortex flows are at similar span locations, the distributions have similar shapes, and the suction pressure levels are of comparable magnitude at M.S. 20.40 and 25.50. The pressure distributions are somewhat misleading, however, since the LVS images clearly reveal a complex, nonconical flow field characterized by multiple, interacting vortices.

The LVS flow visualization in figures 11(a) – 11(f) indicates that the smaller, co-rotating vortex maintains its identity in the cross-flow patterns over more of the body length and to higher angles of attack compared to the results obtained at M_∞ = 0.90 in the previous section. It is conjectured that the difference in the vortex strengths of the interacting vortices is not as great at M_∞ = 1.20 and, consequently, the forebody vortex does not dominate the vortex shed from the transition region to the extent observed at the lower Mach number. It was also observed in a frame-by-frame review of the LVS recording that vorticity appears to feed into the smaller vortex along a limited length of the body edge downstream of the leading-edge break point. If this does, indeed, occur, then this vortex would be more likely to coexist with the primary forebody vortical flow.

The rate of increase of the maximum vortex-induced suction pressure levels at this supersonic free-stream Mach number is modest compared to the results obtained at M_∞ = 0.70 and 0.90. The maximum suction pressure coefficient at M.S. 20.40 is approximately –0.50 at α = 20 degrees and β = 0 degrees, which is approximately 50 percent of the vacuum limit ($C_{p,v} = -0.992$). Pressure measurements that were obtained up to higher angles of attack in a separate phase of this experiment indicate that the maximum suction pressure coefficient at α = 24 degrees is about –0.54, or 54 percent of the vacuum limit. These values are consistent with the results presented in reference 15, which indicated that the maximum suction pressure coefficient on the upper surface of thick delta wings slowly approached a limiting value greater than 90 percent of the vacuum pressure coefficient at low supersonic Mach numbers. Based on the trends presented in reference 15, the slender missile model at M_∞=1.20 requires a much higher angle of attack in order to approach a limiting suction pressure value.

A feature of the PSP images that was noted in the previous section at M_∞ = 0.90 was the absence of red-coded pressure coefficients about the body centerline in the transition region. A similar region is observed in the processed PSP images at M_∞ = 1.20 in figures 11(a) – 11(f), but this region is shifted aft and is more extensive compared to M_∞ = 0.90. The flow recompression along the afterbody, and the concurrent appearance of red-coded pressure coefficients, are delayed as a result of increasing the Mach number. Another contributing factor may be the hypothesized persistence of the vorticity feeding mechanism aft of the planform break, which allows the vortex system to grow in size and strength.

The PSP and ESP pressure measurements at α = 20 degrees and β = -2.5 degrees are compared in figure 11(g). Both techniques correctly capture the qualitative effect of sideslip on the vortex-induced pressure signatures. Reasonable quantitative agreement between the PSP and ESP measurements is obtained on the windward side of the body, where the vortex system is stronger and induces more pronounced suction pressure peaks. In addition, both techniques reveal the apparent presence of a second, co-rotating vortex, which is inferred from the second pressure peak situated closer to the windward leading edge at M.S. 25.50. Less

satisfactory agreement is obtained on the leeward side, where the PSP measurements again tend to overestimate the leeward vortex pressure signature, particularly at M.S. 30.00. The processed PSP image clearly shows the pressure footprint of the windward vortex along the entire exposed body length, denoted by a narrow band of blue color situated to the left of the body centerline. There is also evidence of a region of high suction pressures closer to the windward leading edge along the transition region of the body. A much fainter vortex footprint is observed on the leeward side of the forebody, but this footprint is not discernible along the afterbody. The latter observation is consistent with the upward migration of the vortical flow that was observed in the LVS images in the previous section at M_∞ = 0.90.

Concluding Remarks

A wind tunnel experiment was conducted in the NASA Langley Research Center 8-Foot Transonic Pressure Tunnel using pressure-sensitive paint and electronically-scanned pressure measurement techniques to quantify the vortex-induced surface pressure field on a faceted, sharp leading-edge missile model at subsonic and transonic speeds. This experiment was the first application of a dedicated PSP system using a scientific-grade digital imaging system at the 8-Foot TPT and was the precursor to the PSP system in current use at the NASA LaRC supersonic Unitary Plan Wind Tunnel. The interpretation of the PSP and ESP pressure measurements was augmented by off-surface flow visualization images obtained in a separate phase of the experiment using a laser vapor screen technique. The testing was performed at free-stream Mach numbers of 0.70, 0.90, and 1.20 and a Reynolds number of 3.0 million per foot, and pressure measurements were acquired at moderate to high angles of attack and at zero and nonzero sideslip angles. Global calibrations of the PSP images were obtained at all test conditions using the ESP data obtained at the discrete pressure tap locations. Satisfactory quantitative agreement was generally obtained between the PSP and ESP measurement techniques at all combinations of the Mach number, angle of attack, and angle of sideslip. The largest differences in the measured pressure coefficient were observed at the most aft measurement station on the model afterbody, where the PSP technique overestimated the vortex suction pressure levels on one side of the body because of an asymmetric pressure field response. This asymmetry was not apparent in the ESP tap data or the LVS images and was attributed to possible anomalies in the thickness distribution of the PSP and base coating, nonuniform UV illumination, and/or nonuniform photodegradation. Despite these discrepancies, the relative error between the PSP and ESP pressure measurements was less than 1 percent at M_∞ = 0.70 and less than 3 percent at M_∞ = 0.90 and 1.20. Both techniques effectively captured the vortex-induced pressure signatures at all measurement stations. The PSP and ESP pressure distributions and the processed PSP images showing the global surface pressure response were consistent with the vortex cross-flow patterns observed in the LVS flow visualization. The pressure measurement and flow visualization techniques were complementary, since each revealed details of the vortex flow physics that were either unclear or not apparent in the other. The 8-Foot TPT experiment indicated that the PSP technique is a useful tool to obtain quantitative and qualitative information on the surface pressure field response on a complex aerodynamic shape at subsonic and transonic speeds.

References

1. McLachlan, B. G.; Bell, J. H.; Kennelly, R. A.; Schreiner, J. A.; Smith, S. C.; Strong, J. M.; Gallery, J.; and Gouterman, M.: Pressure Sensitive Paint Use in the Supersonic High-Sweep Oblique Wing (SHOW) Test. AIAA-92-2686, June 1992.

2. McLachlan, B. G.; and Bell, J. H.: Pressure-Sensitive Paint in Aerodynamic Testing. *Experimental Thermal and Fluid Science*, Vol. 10, 1995, pp. 470-485.

3. Erickson, G. E.: Overview of Selected Measurement Techniques for Aerodynamics Testing in the NASA Langley Unitary Plan Wind Tunnel. AIAA-2000-2396, June 2000.

4. Braslow, A. L.; Hicks, R. M.; and Harris, R. V., Jr.: *Use of Grit-Type Boundary-Layer Transition Strips on Wind-Tunnel Models*. NASA TN D-3579, 1966.

5. Brooks, C. W., Jr.; Harris, C. D.; and Reagon, P. G.: *The NASA Langley 8-Foot Transonic Tunnel Calibration*. NASA TP 3437, 1994.

6. Trosin, J.; and Hermstad, D.: *PAINTCP V2.3 User's Guide*. TN-94-8006-0000-48, Technical Note No. 48, Revision 1, NASA Ames Research Center, May 1995.

7. Erickson, G. E.; and Inenaga, A. S.: *Fiber-Optic-Based Laser Vapor Screen Flow Visualization for Aerodynamic Research in Larger Scale Subsonic and Transonic Wind Tunnels*. NASA TM 4514, 1994.

8. Jagharghi, A. J.; Cler, D. L.; Erickson, G. E.; Mitchell, M.; Lamb, M.; Gibson, L.S.; Farokhi, S.; Taghavi, R. R.; and Hazlewood, R.: Application of Pressure Sensitive Paint to Measurement of Global Surface Pressure for a Convergent-Divergent Nozzle and an Isolated Double Delta Wing at Transonic Speeds. AIAA-95-0639, January 1995.

9. Oglesby, D. M.; Puram, C. K.; and Upchurch, B. T.: *Optimization of Measurements with Pressure Sensitive Paints*. NASA TM 4695, 1995.

10. Erickson, G. E.: *Wind Tunnel Investigation of the Interaction and Breakdown Characteristics of Slender-Wing Vortices at Subsonic, Transonic, and Supersonic Speeds*. NASA TP 3114, 1991.

11. Erickson, G. E.; and Murri, D. G.: *Wind Tunnel Investigations of Forebody Strakes for Yaw Control on F/A-18 Model at Subsonic and Transonic Speeds*. NASA TP 3360, 1993.

12. Wood, R. L.; Wilcox, F. J., Jr.; Bauer, S.X.S.; and Allen, J. M.: *Vortex Flows at Supersonic Speeds*. NASA TP-2003-211950, 2003.

13. Campbell, J. F.; and Chambers, J. R.: *Patterns in the Sky – Natural Visualization of Aircraft Flow Fields*. NASA SP-514, 1994.

14. Hemsch, M. J.; and Luckring, J. M.: Connection Between Leading-Edge Vortex Lift, and Vortex Strength for Delta Wings. *J. Aircr*., vol. 27, no. 5, May 1990, pp. 473-475.

15. Wood, R. M.: *Supersonic Aerodynamics of Delta Wings*. NASA TP 2771, 1988.

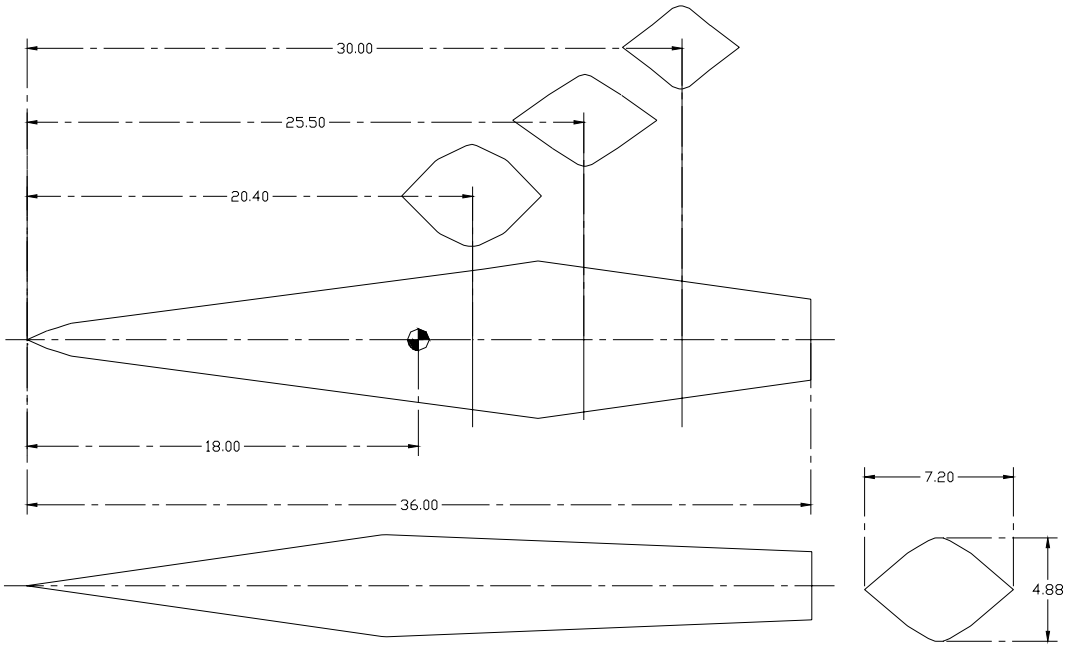

Figure 1. Dimensional details of the faceted missile model. (All dimensions are in inches.)

Figure 2. Faceted missile model installed in the test section of the NASA LaRC 8-Foot TPT.

Figure 3. Close-up view of the faceted missile model.

Figure 4. Faceted missile model installed in the test section of the NASA LaRC 8-Foot TPT with PSP applied to the upper surface.

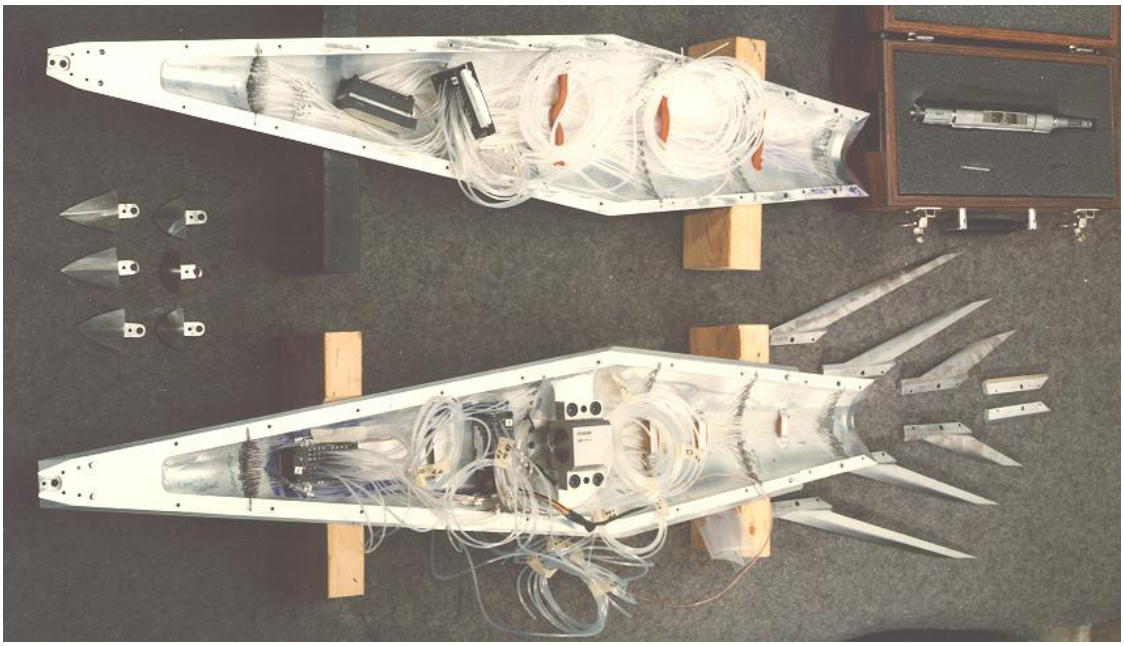

Figure 5. Photograph of the faceted missile model components and instrumentation.

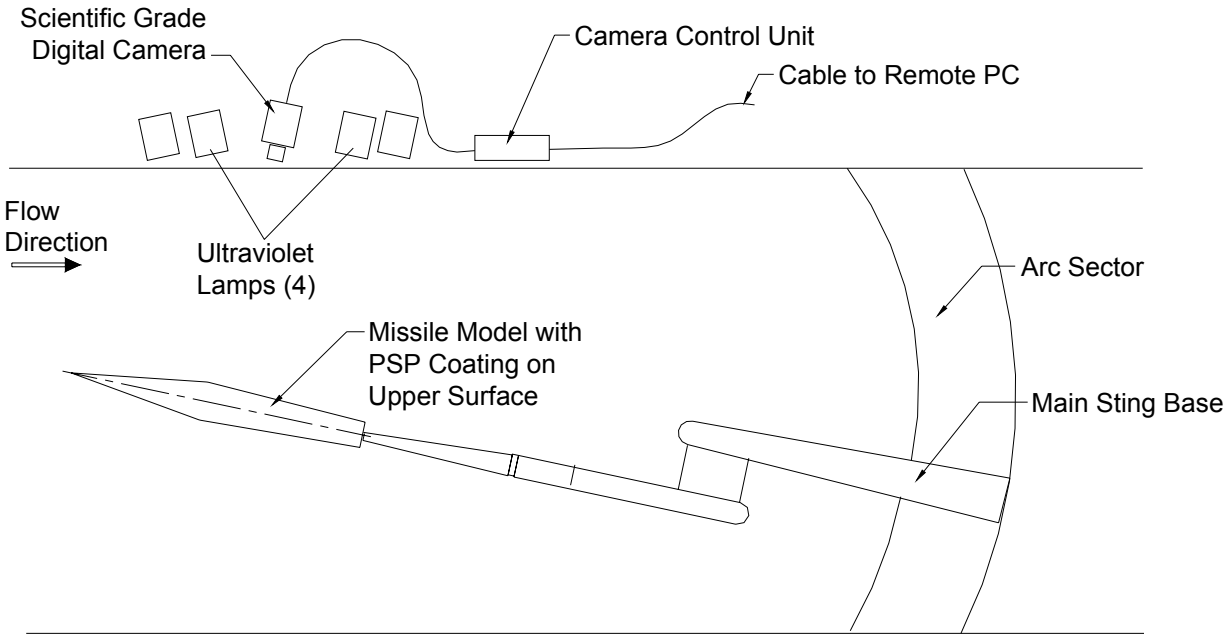

Figure 6. Sketch of the main components of the NASA LaRC 8-Foot TPT PSP system.

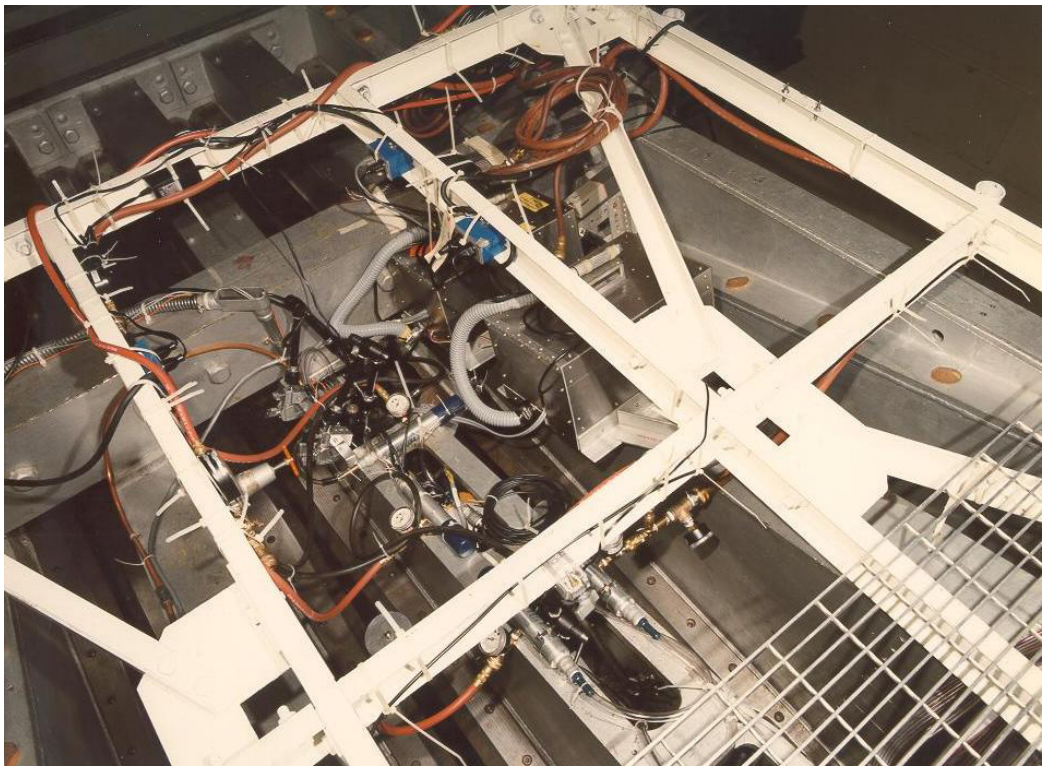

Figure 7. Photograph of the PSP system installation on top of the NASA LaRC 8-Foot TPT test section.

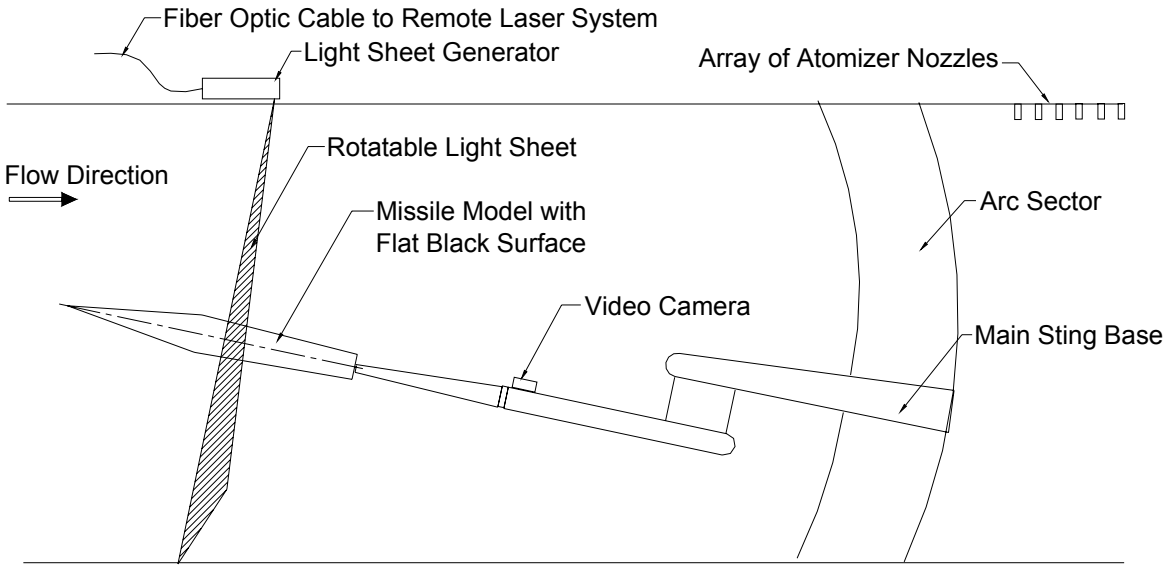

Figure 8. Sketch of the primary fiber optic-based LVS system components in the 8-Foot TPT.

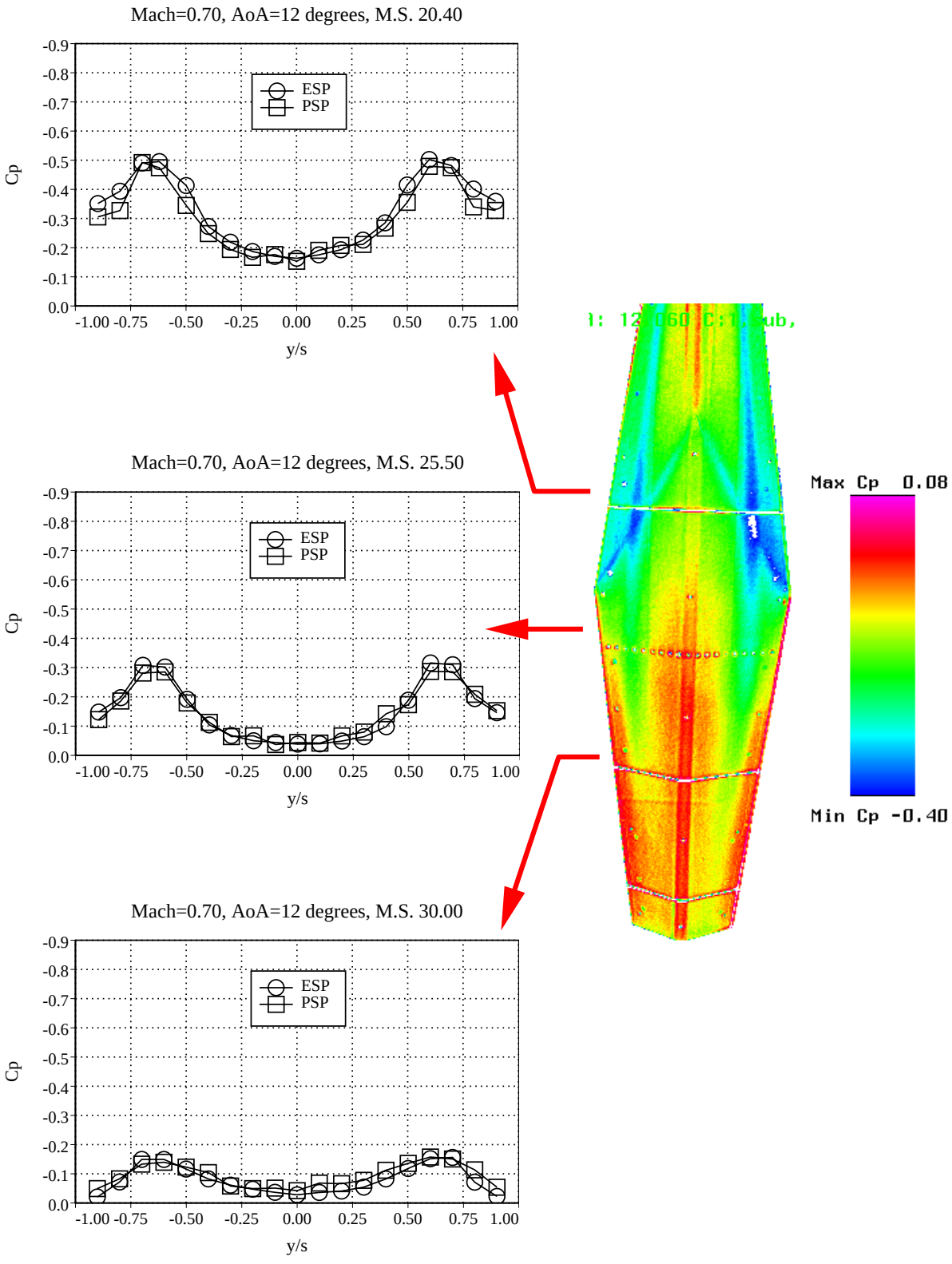

(a) α = 12 degrees.

Figure 9. Comparison of PSP and ESP upper surface static pressure distributions at $M_\infty = 0.70$.

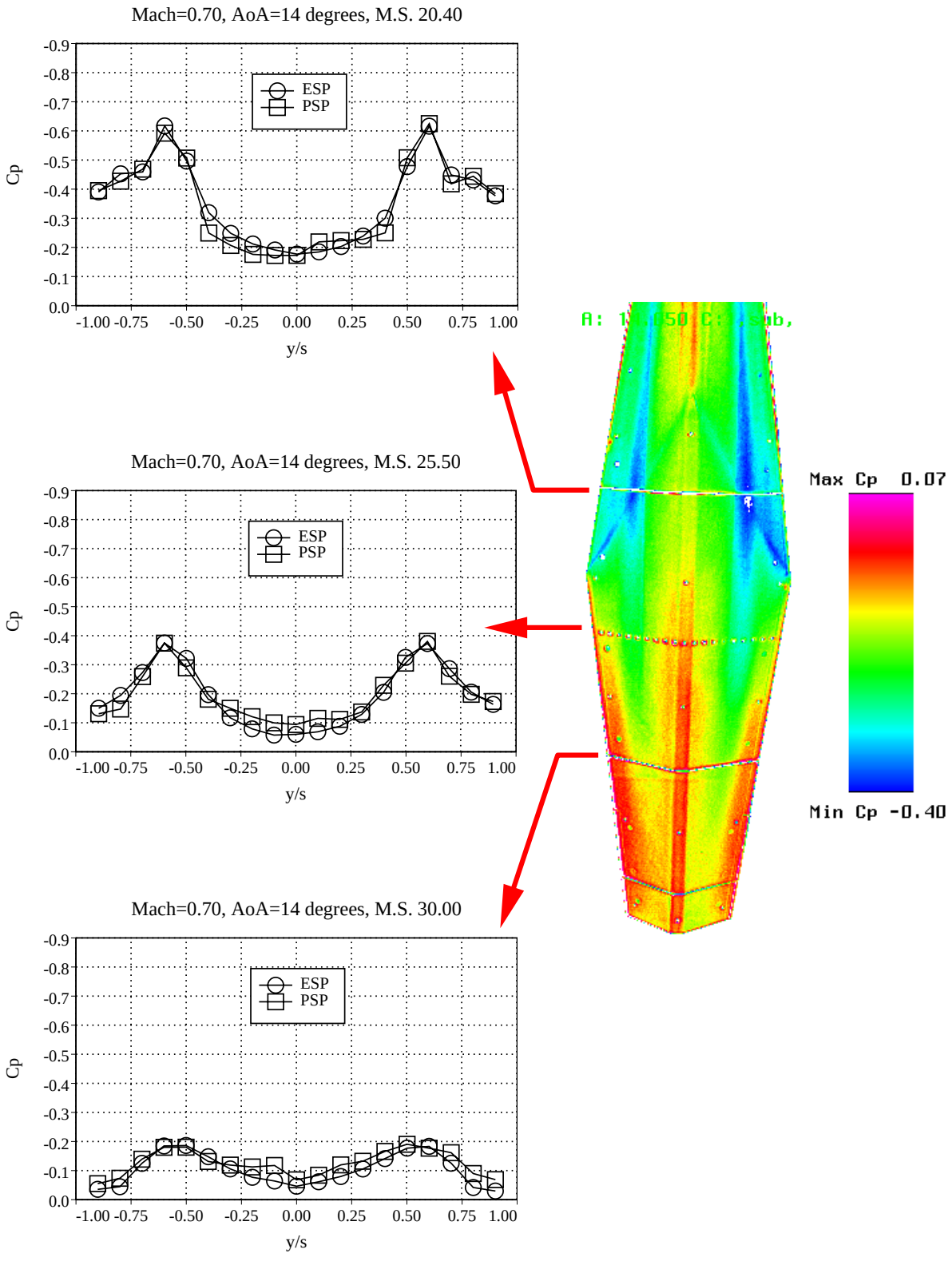

(b) α = 14 degrees.

Figure 9. Continued.

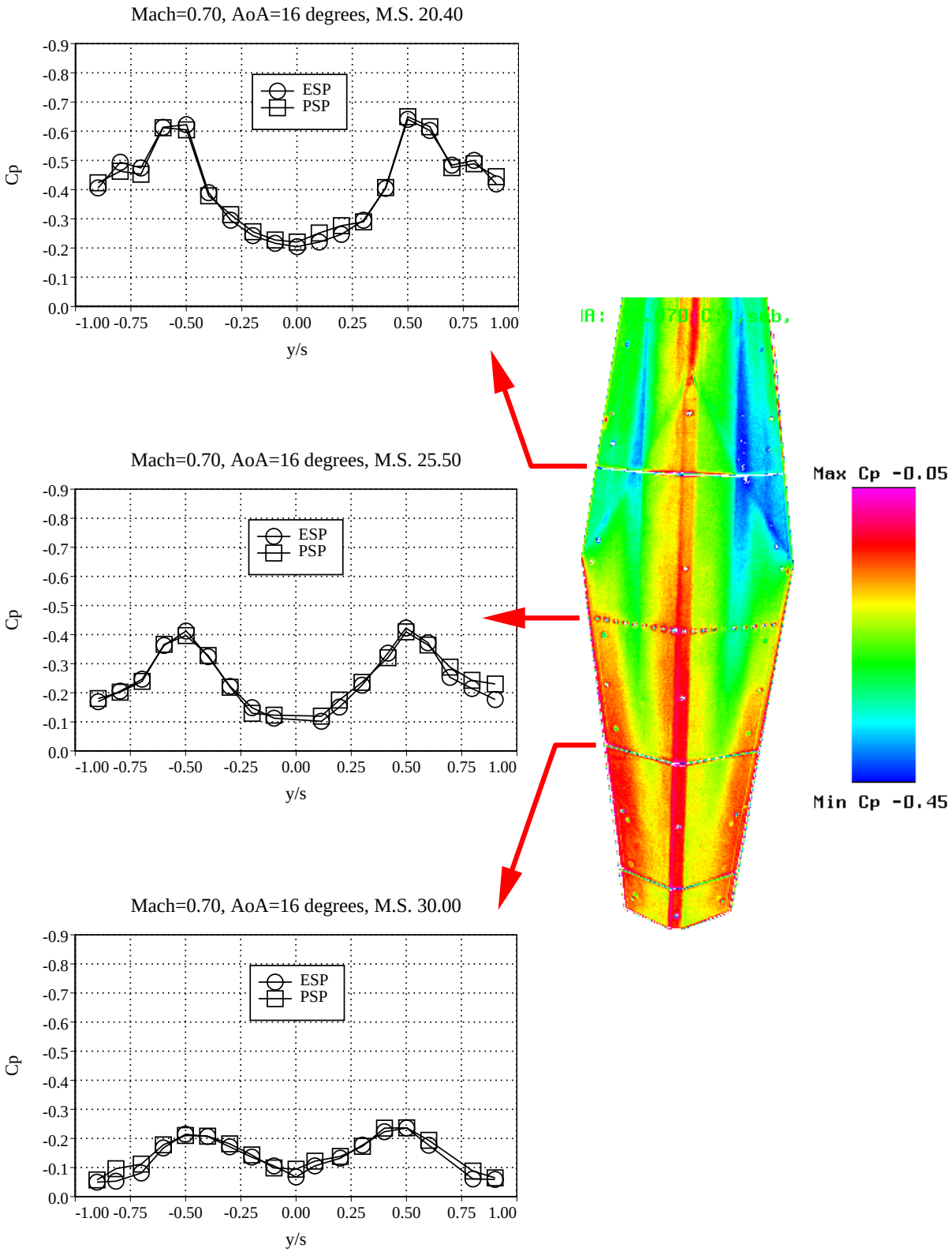

(c) α = 16 degrees.

Figure 9. Continued.

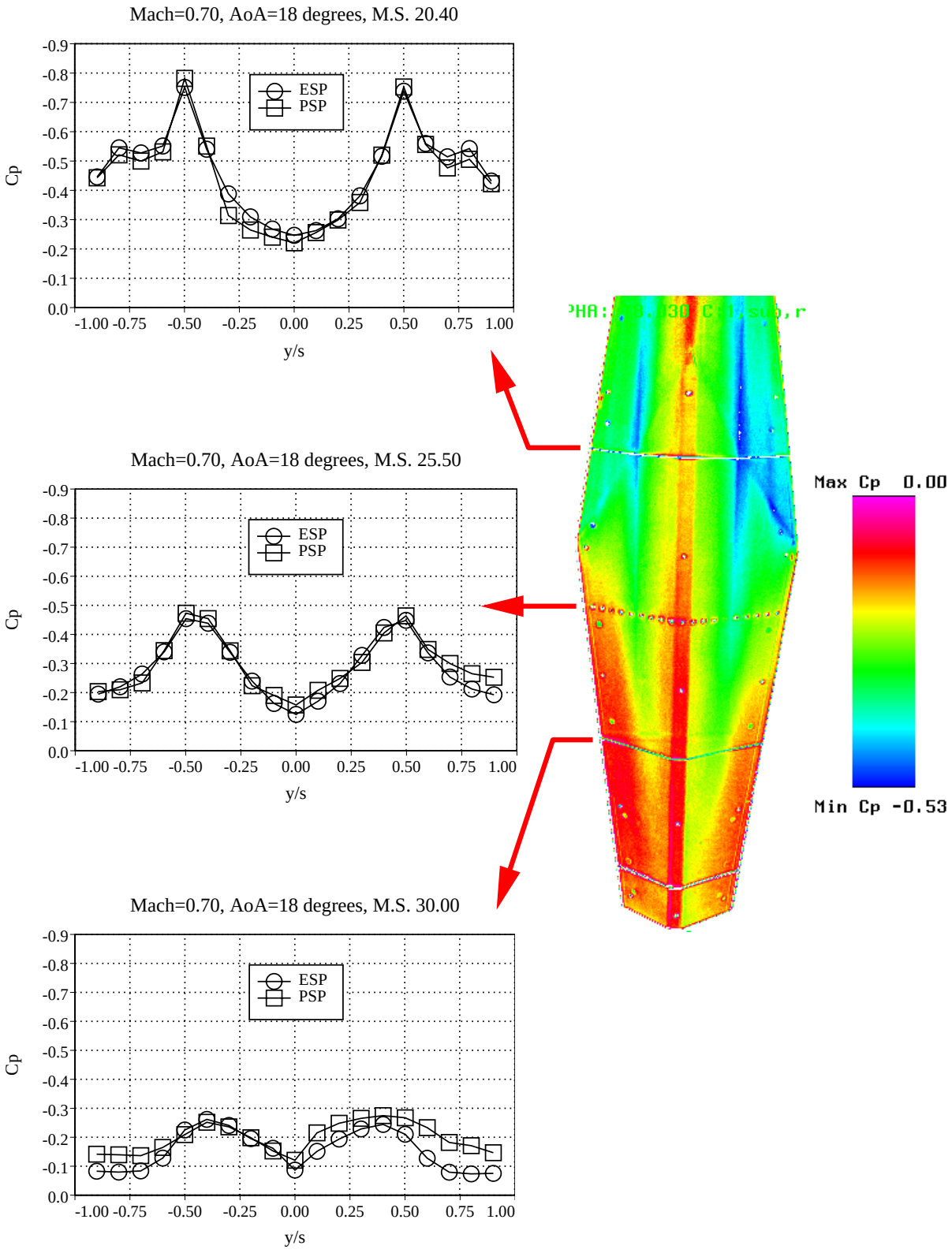

(d) α = 18 degrees.

Figure 9. Continued.

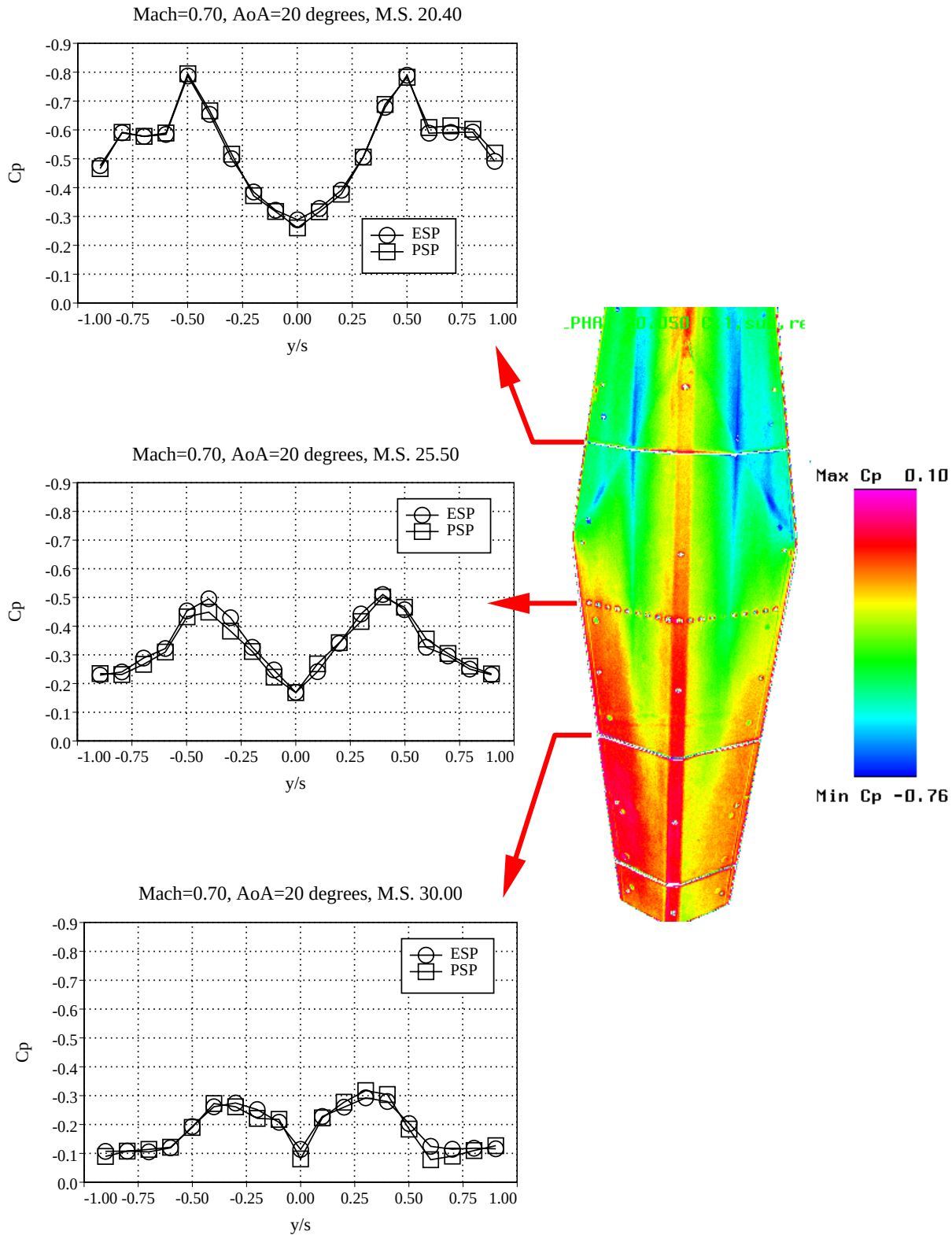

(e) $\alpha = 20$ degrees.

Figure 9. Continued.

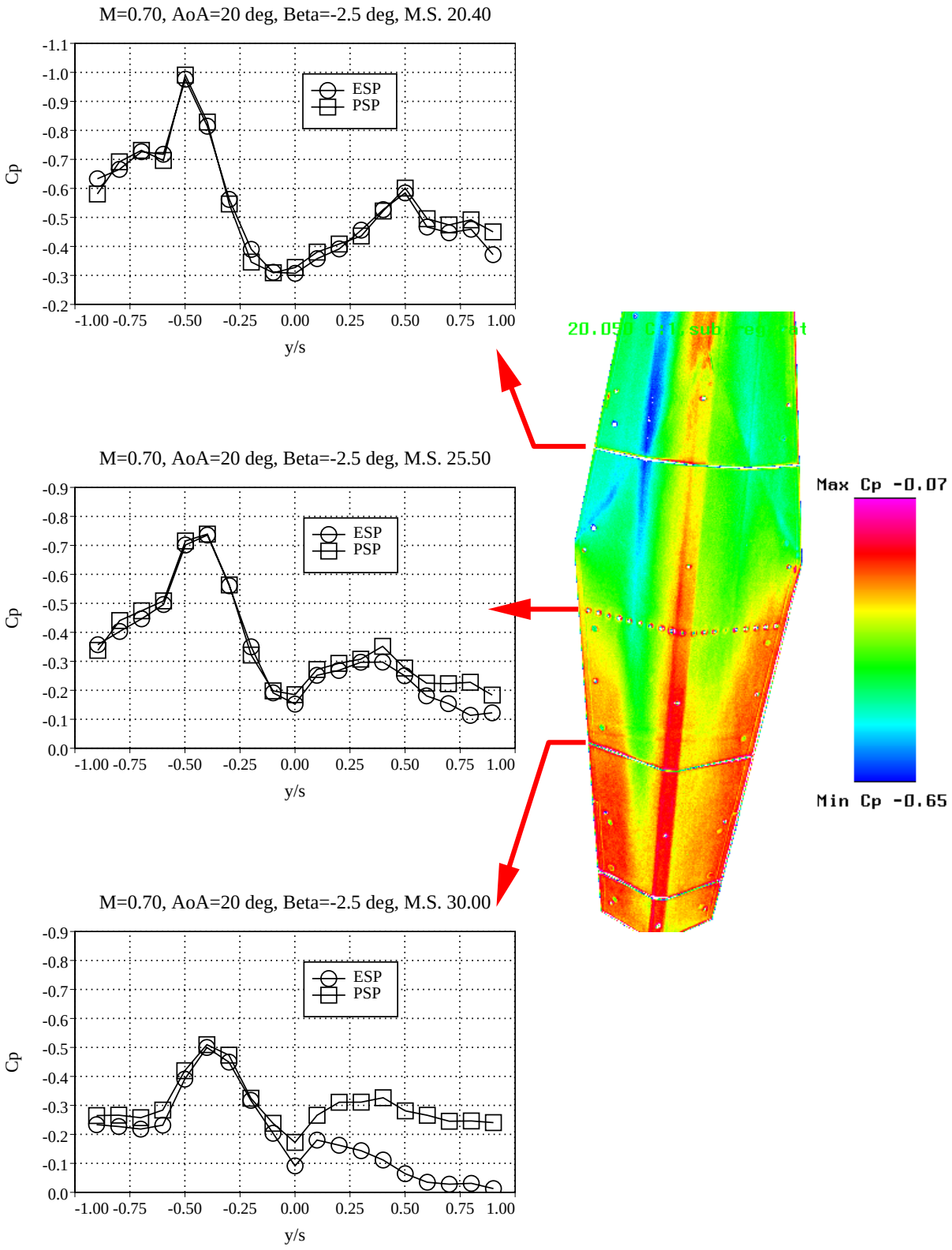

(f) α = 20 degrees, β = -2.5 degrees.

Figure 9. Concluded.

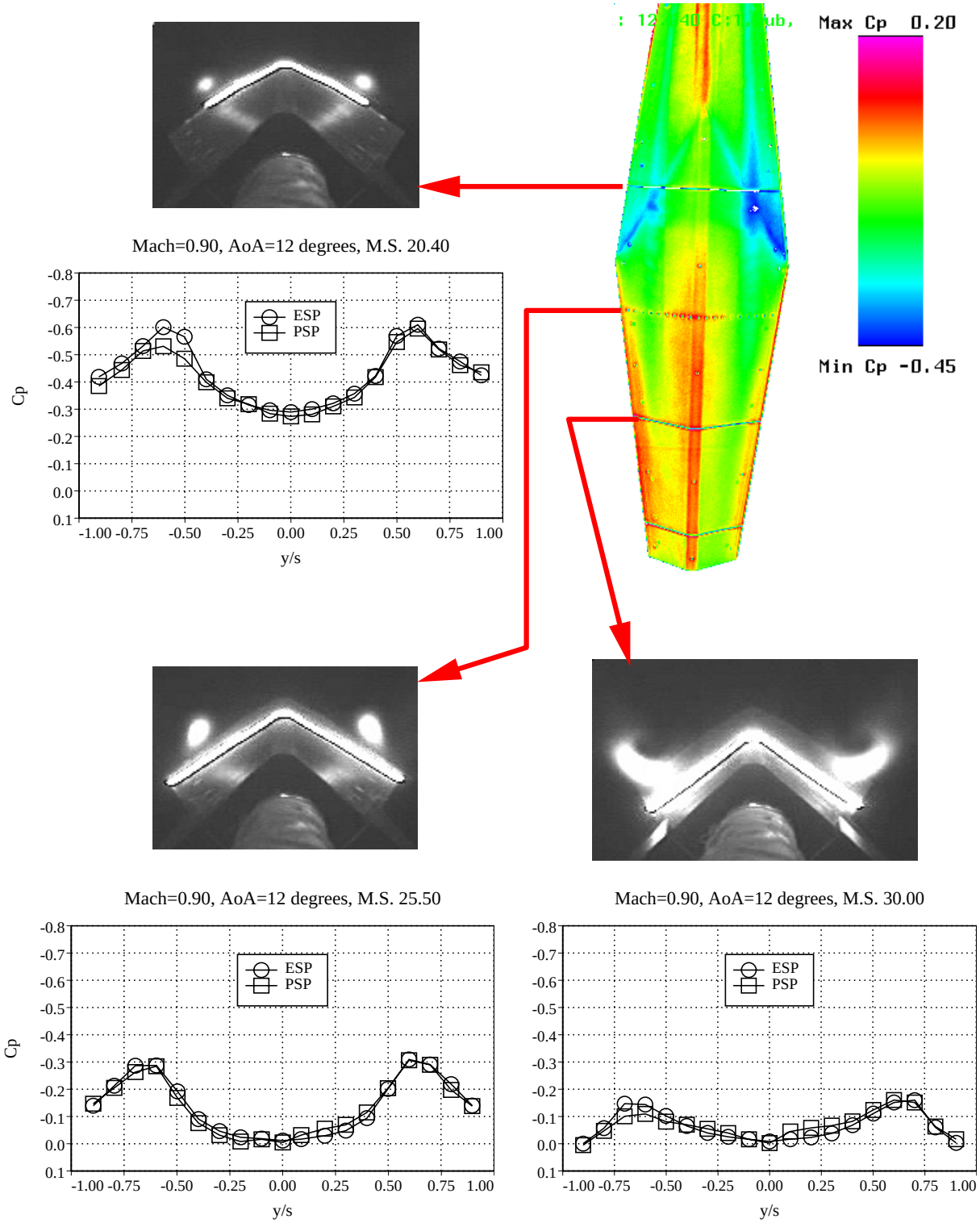

(a) α = 12 degrees.

Figure 10. Composite plots of PSP and ESP pressure measurements and LVS flow visualization at $M_\infty = 0.90$.

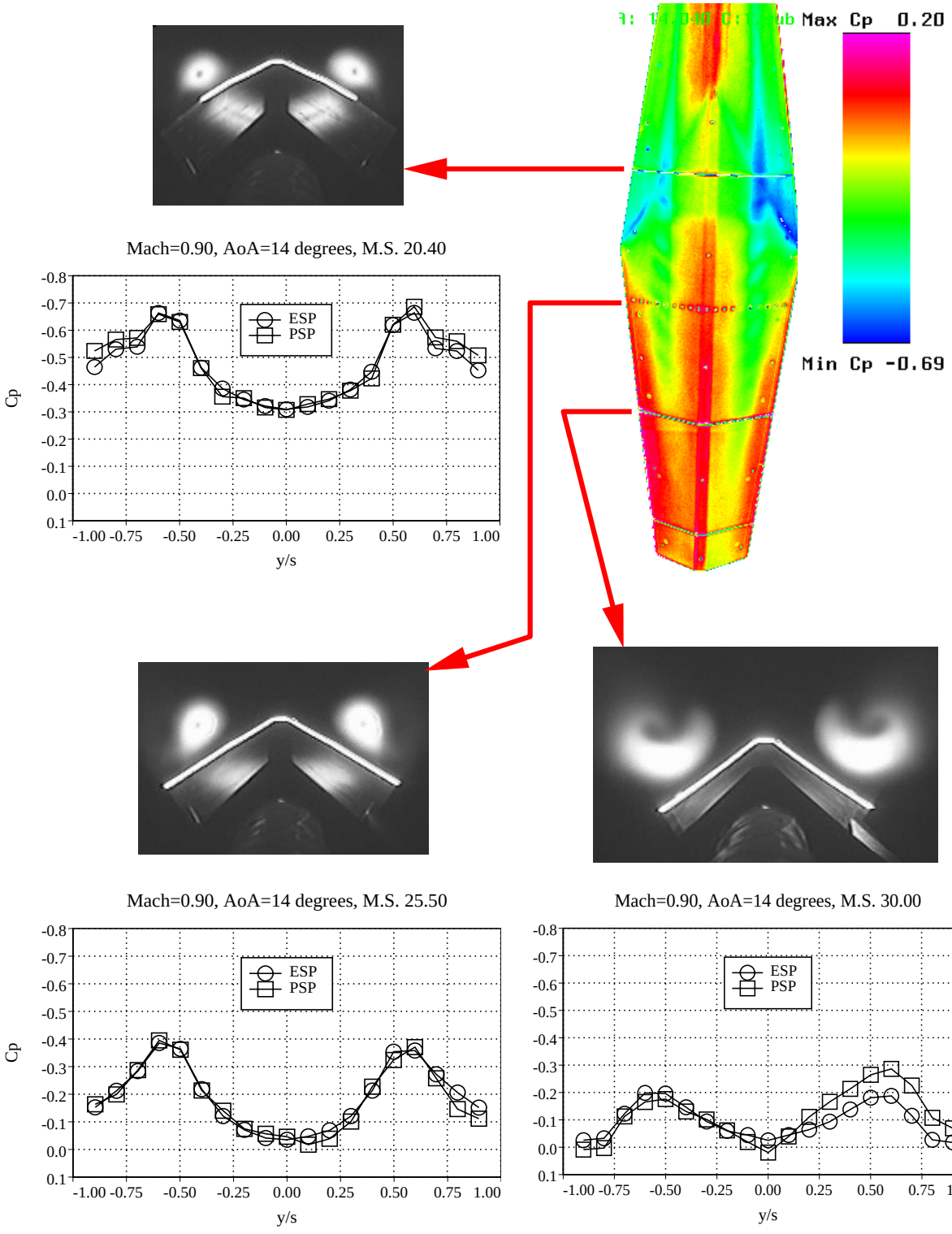

(b) α = 14 degrees.

Figure 10. Continued.

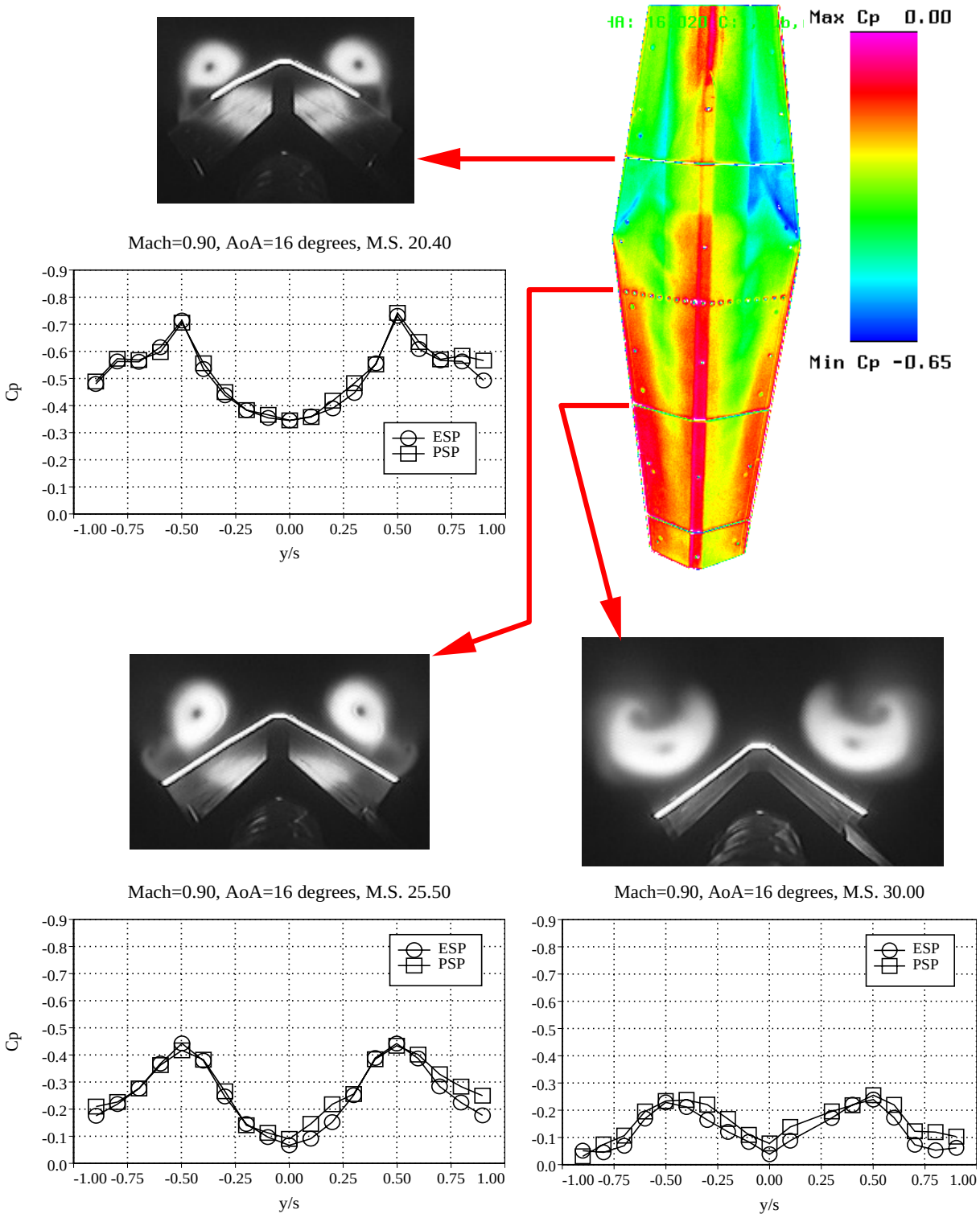

(c) α = 16 degrees.

Figure 10. Continued.

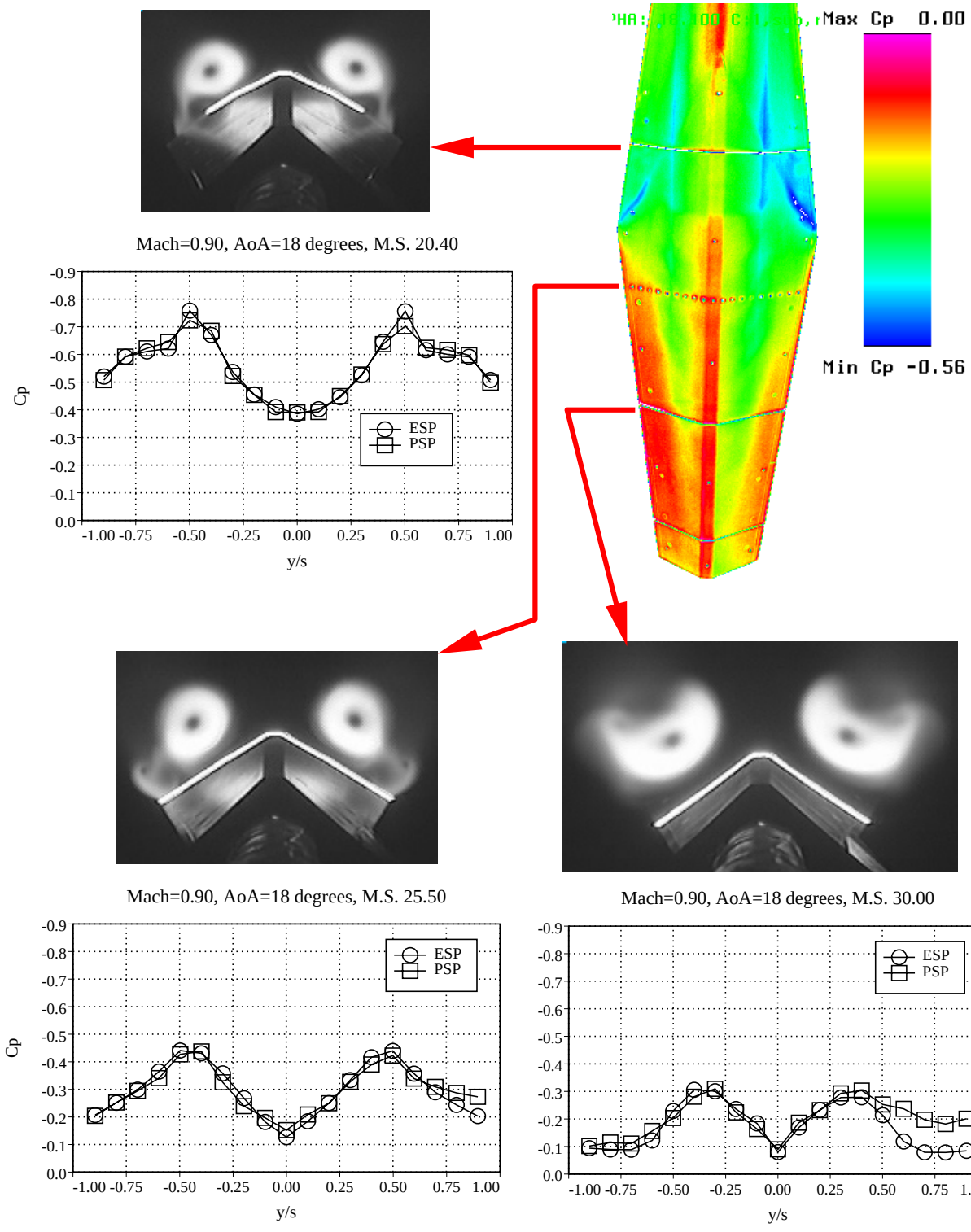

(d) α = 18 degrees.

Figure 10. Continued.

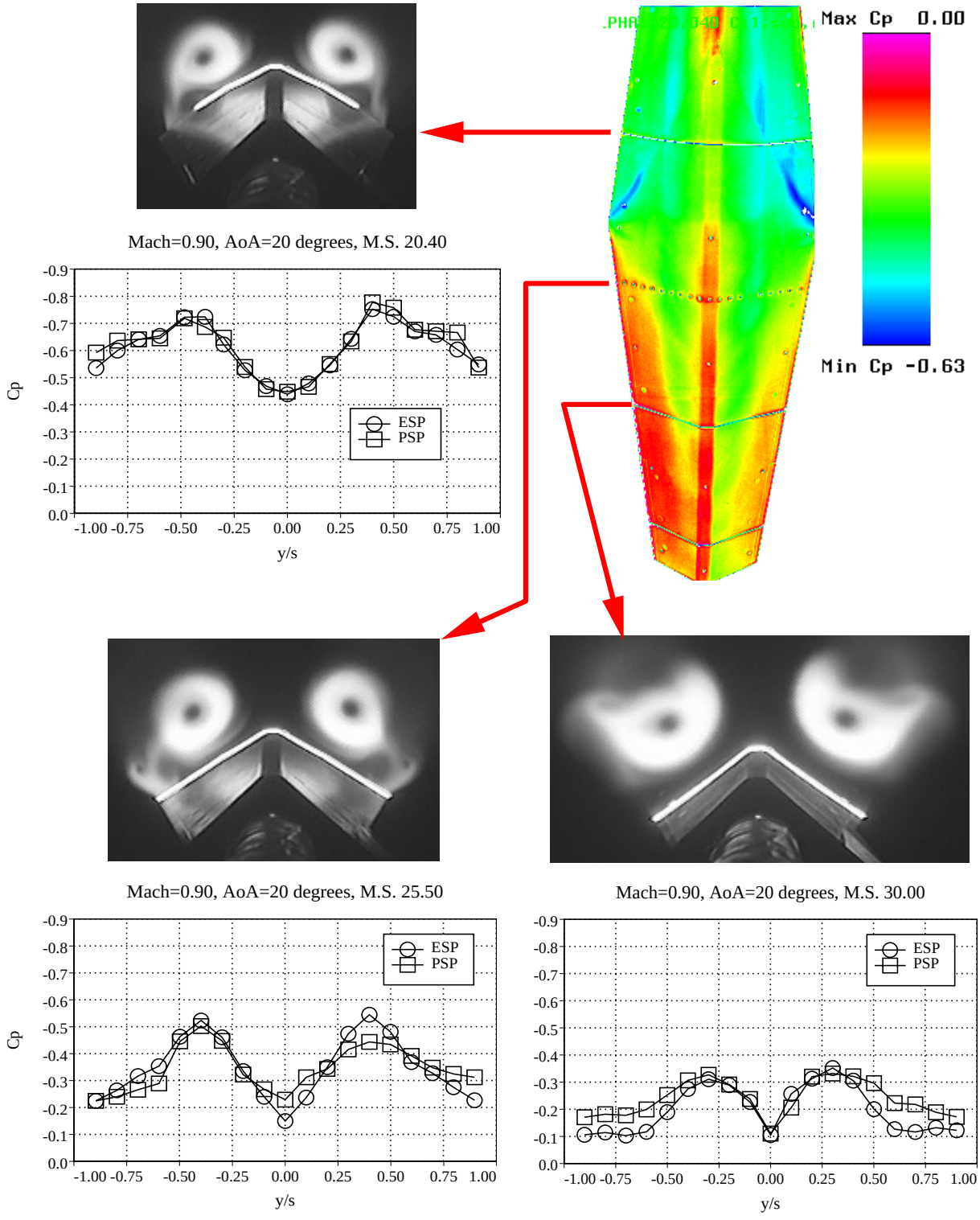

(e) $\alpha = 20$ degrees.

Figure 10. Continued.

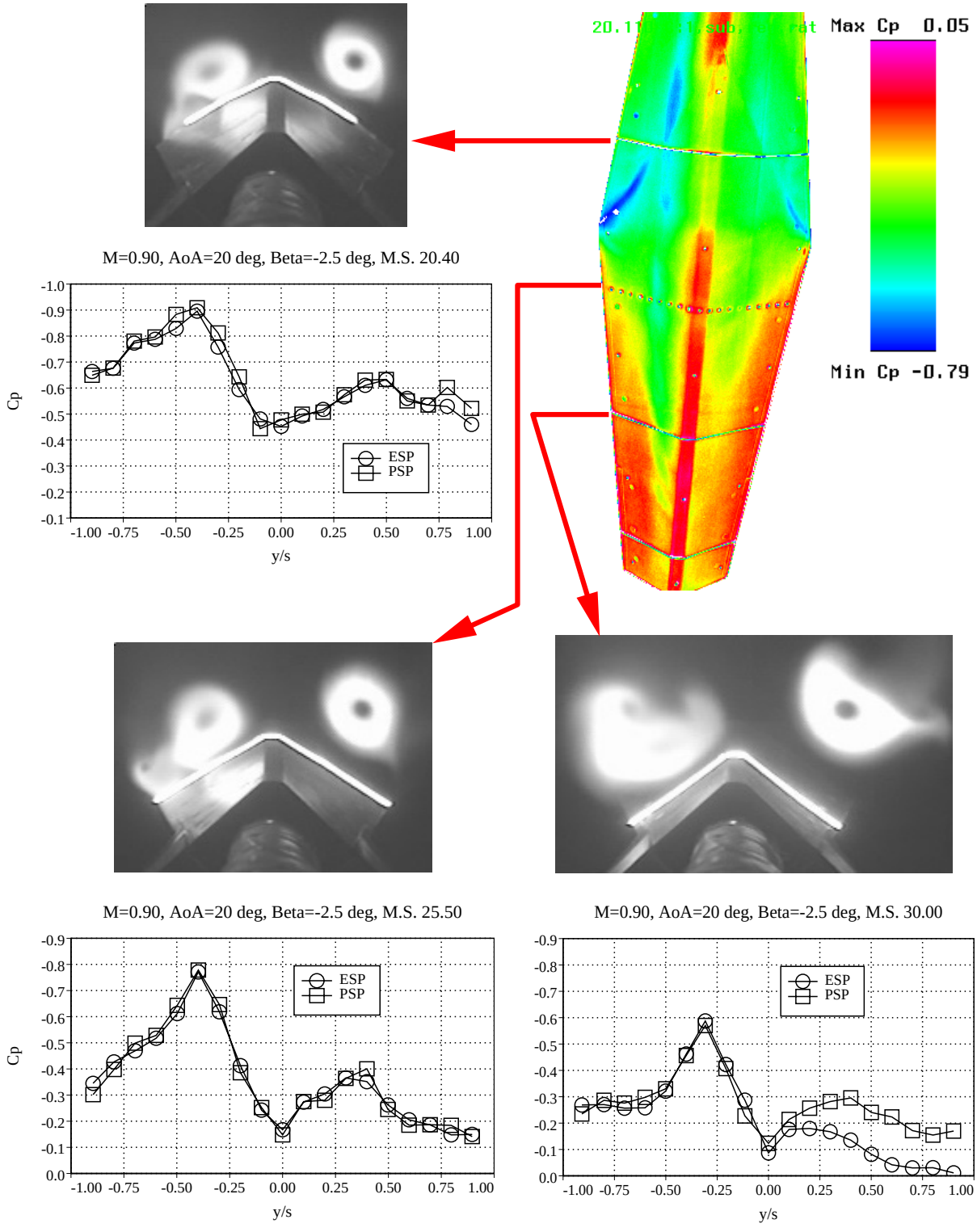

(f) $\alpha = 20$ degrees, $\beta = -2.5$ degrees.

Figure 10. Concluded.

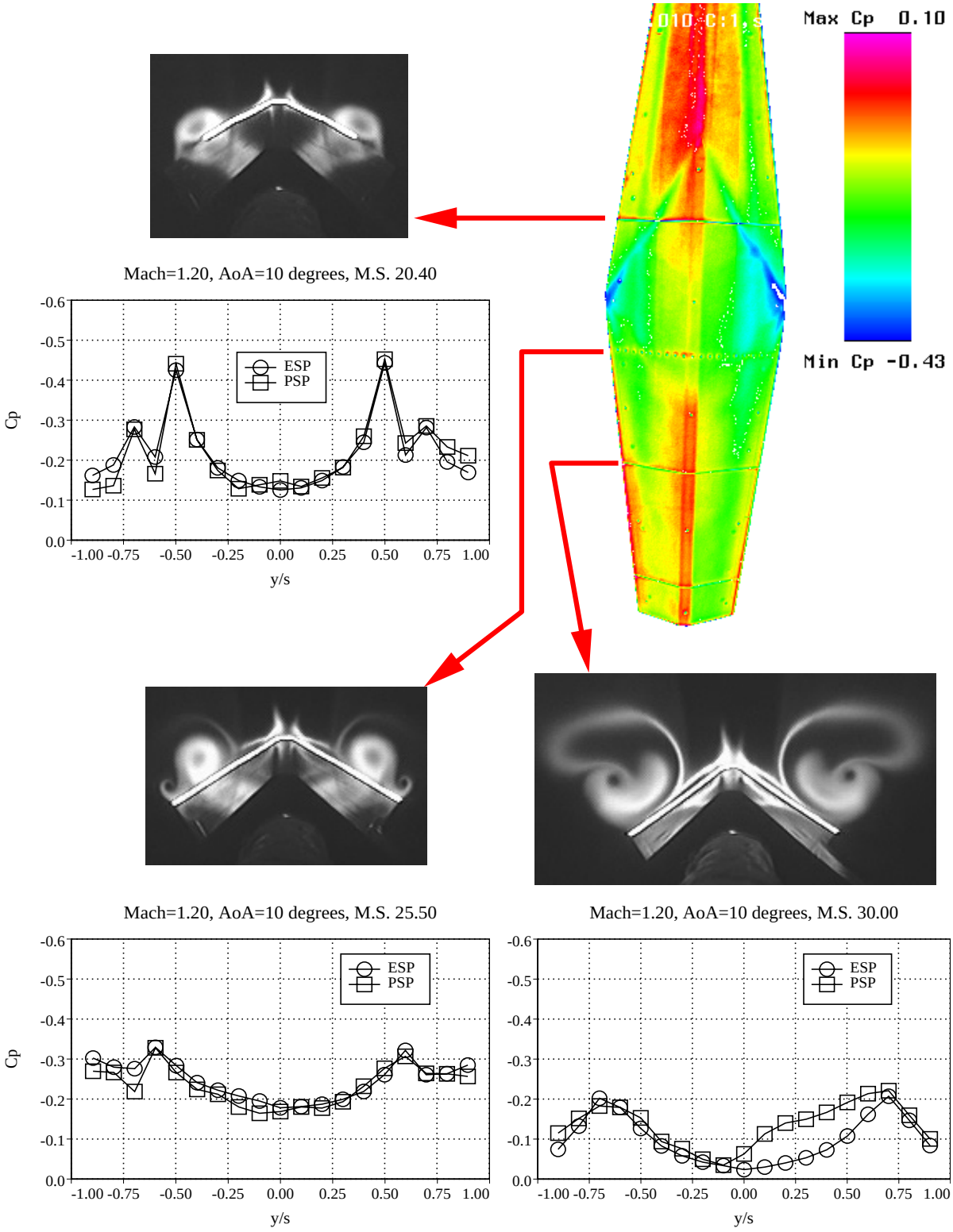

(a) α = 10 degrees.

Figure 11. Composite plots of PSP and ESP pressure measurements and LVS flow visualization at M_∞ = 1.20.

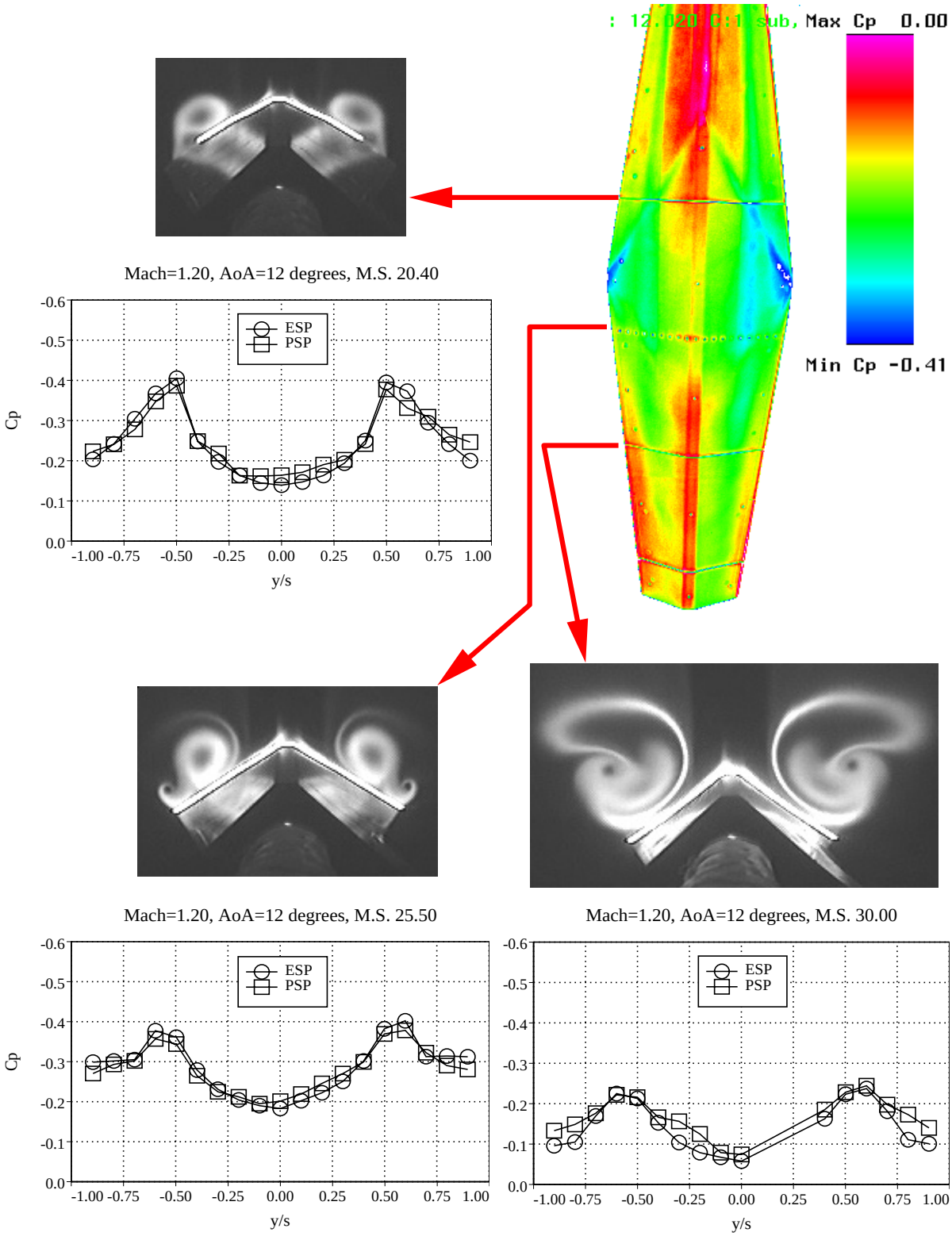

(b) α = 12 degrees.

Figure 11. Continued.

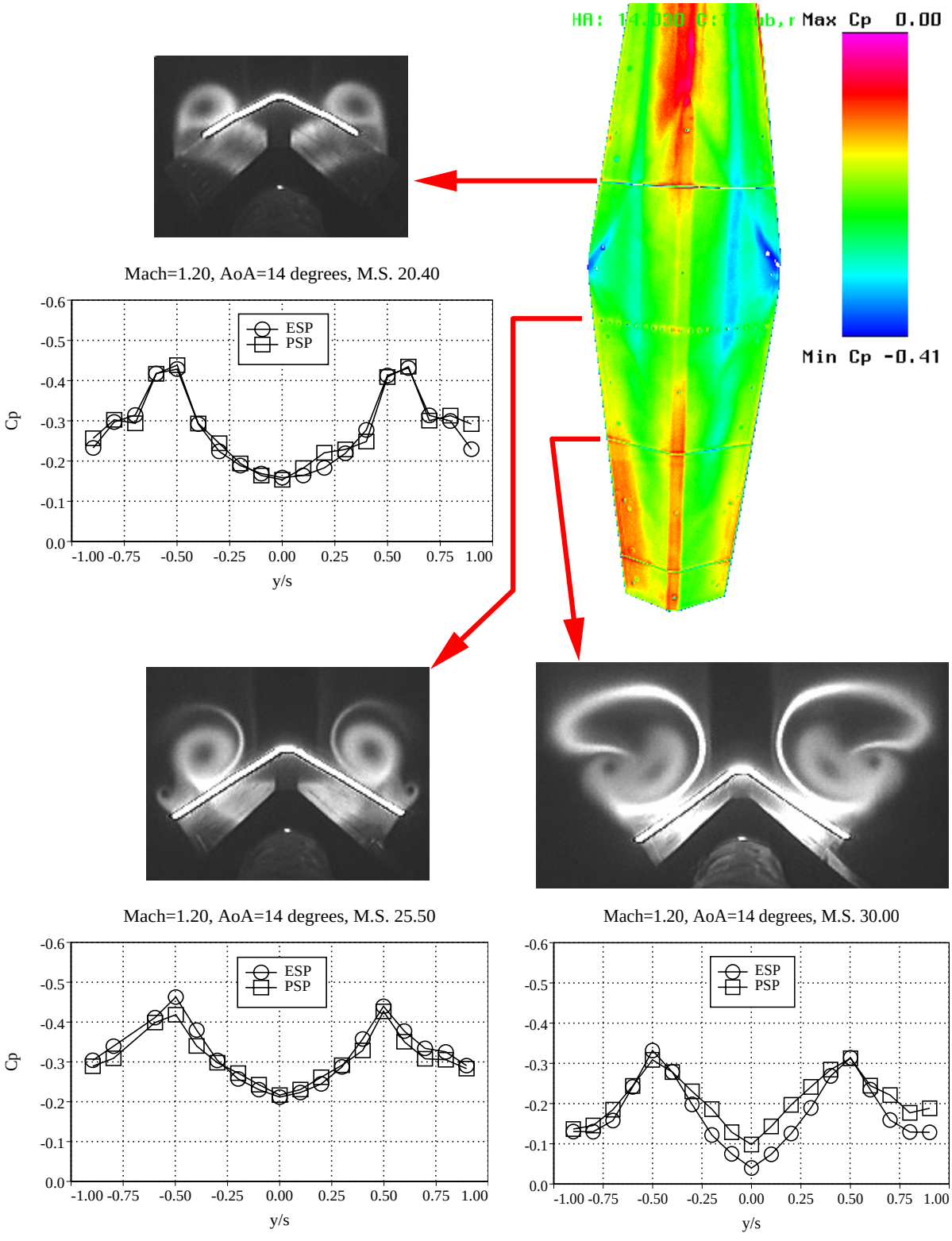

(c) α = 14 degrees.

Figure 11. Continued.

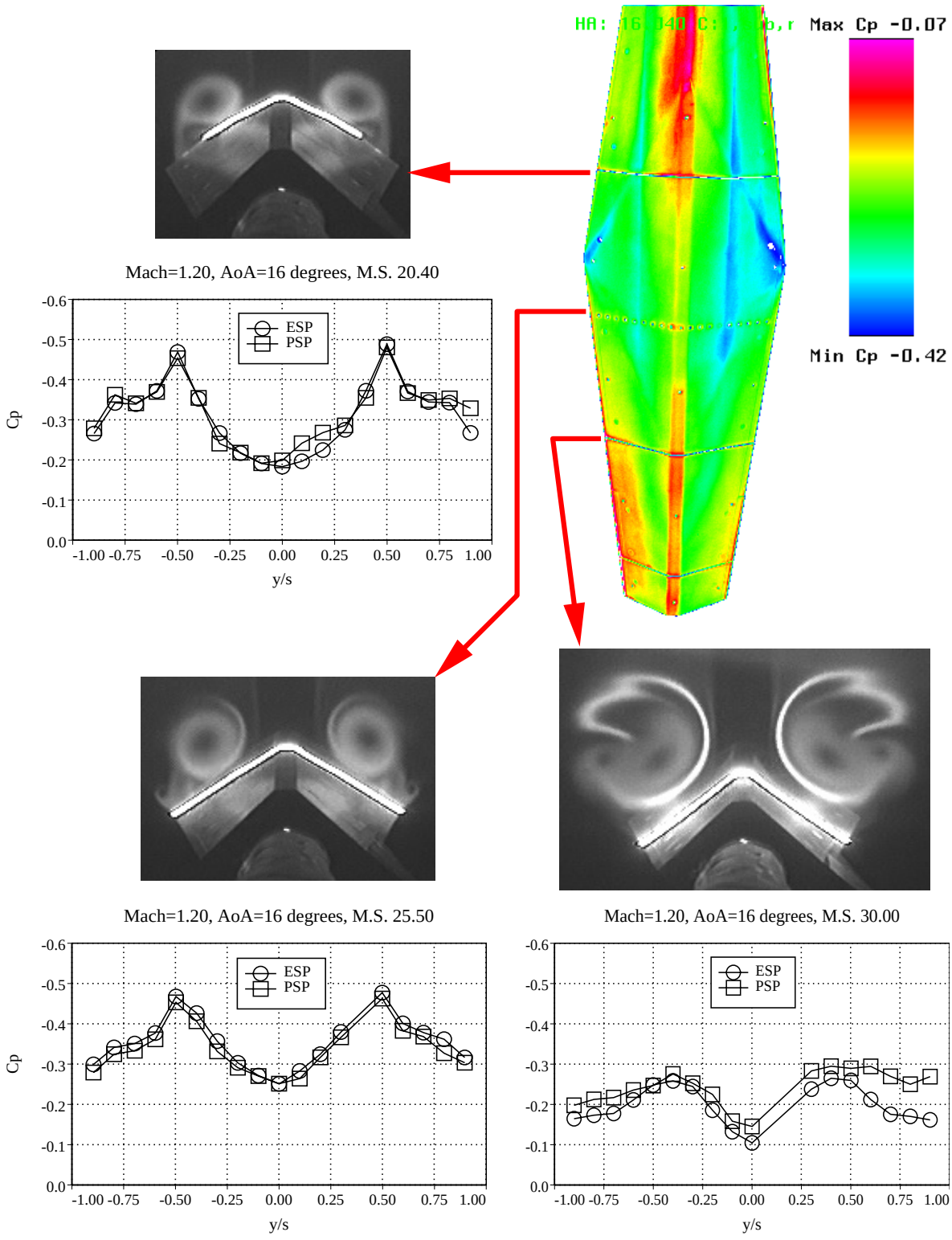

(d) α = 16 degrees.

Figure 11. Continued.

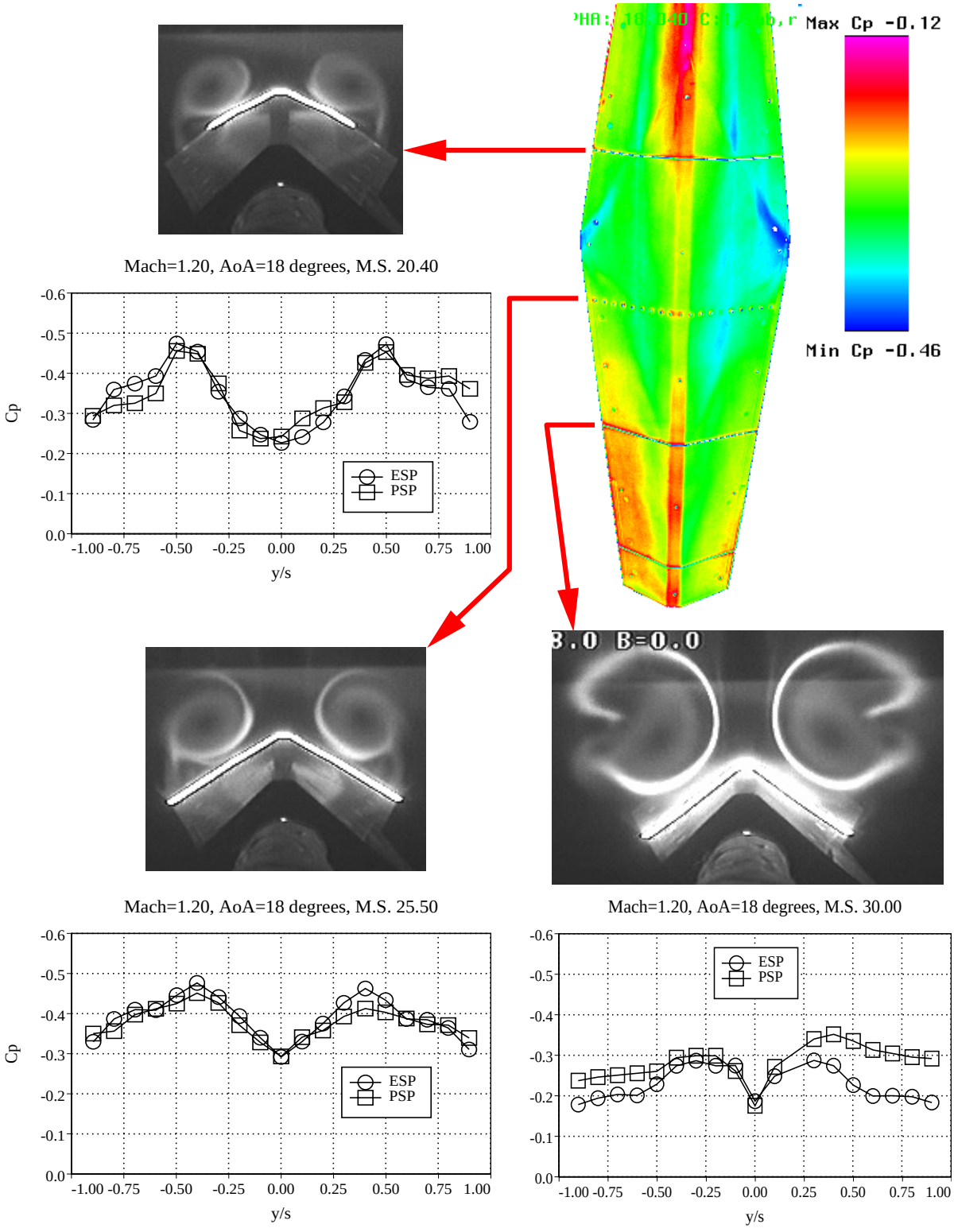

(e) α = 18 degrees.

Figure 11. Continued.

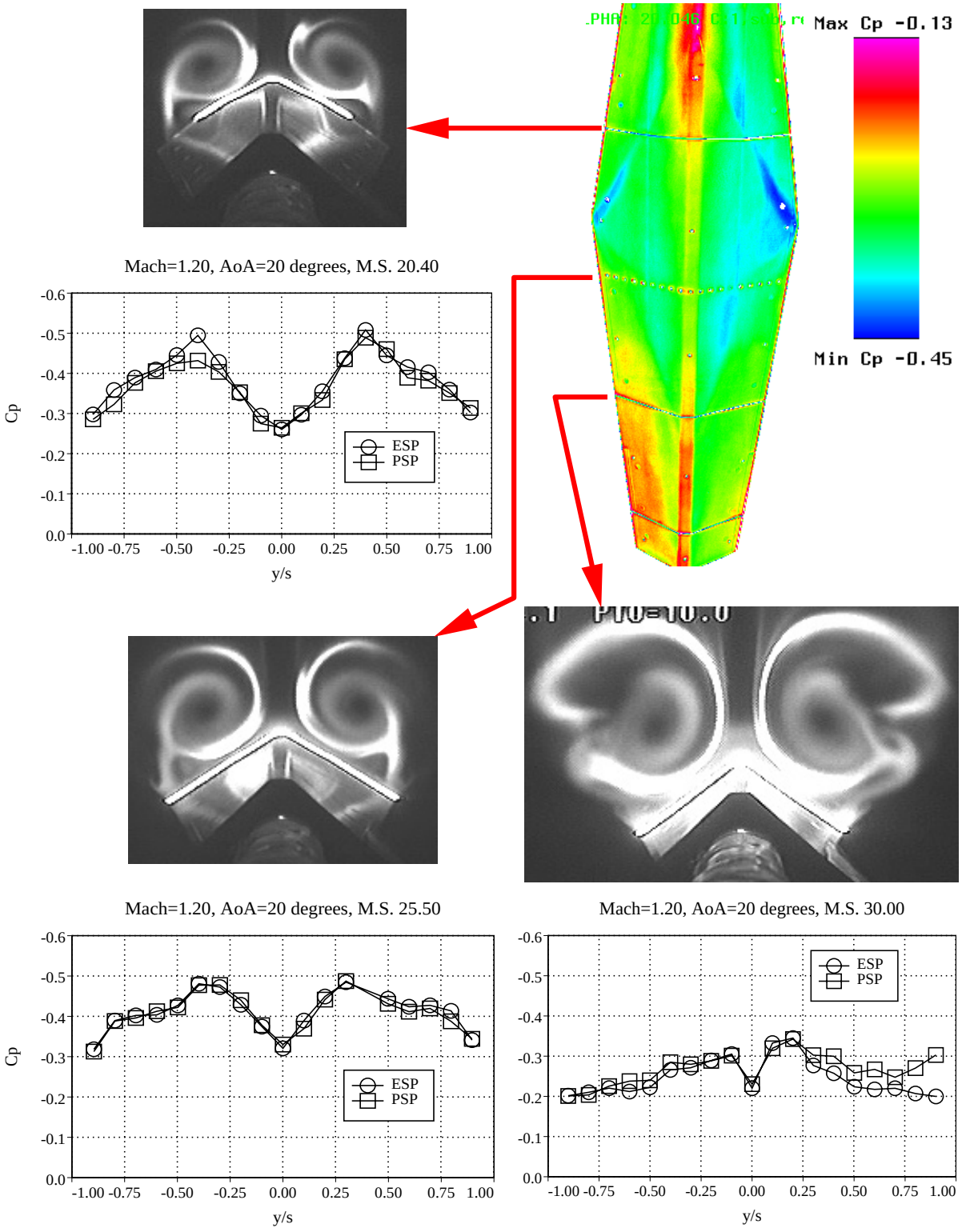

(f) $\alpha = 20$ degrees.

Figure 11. Continued.

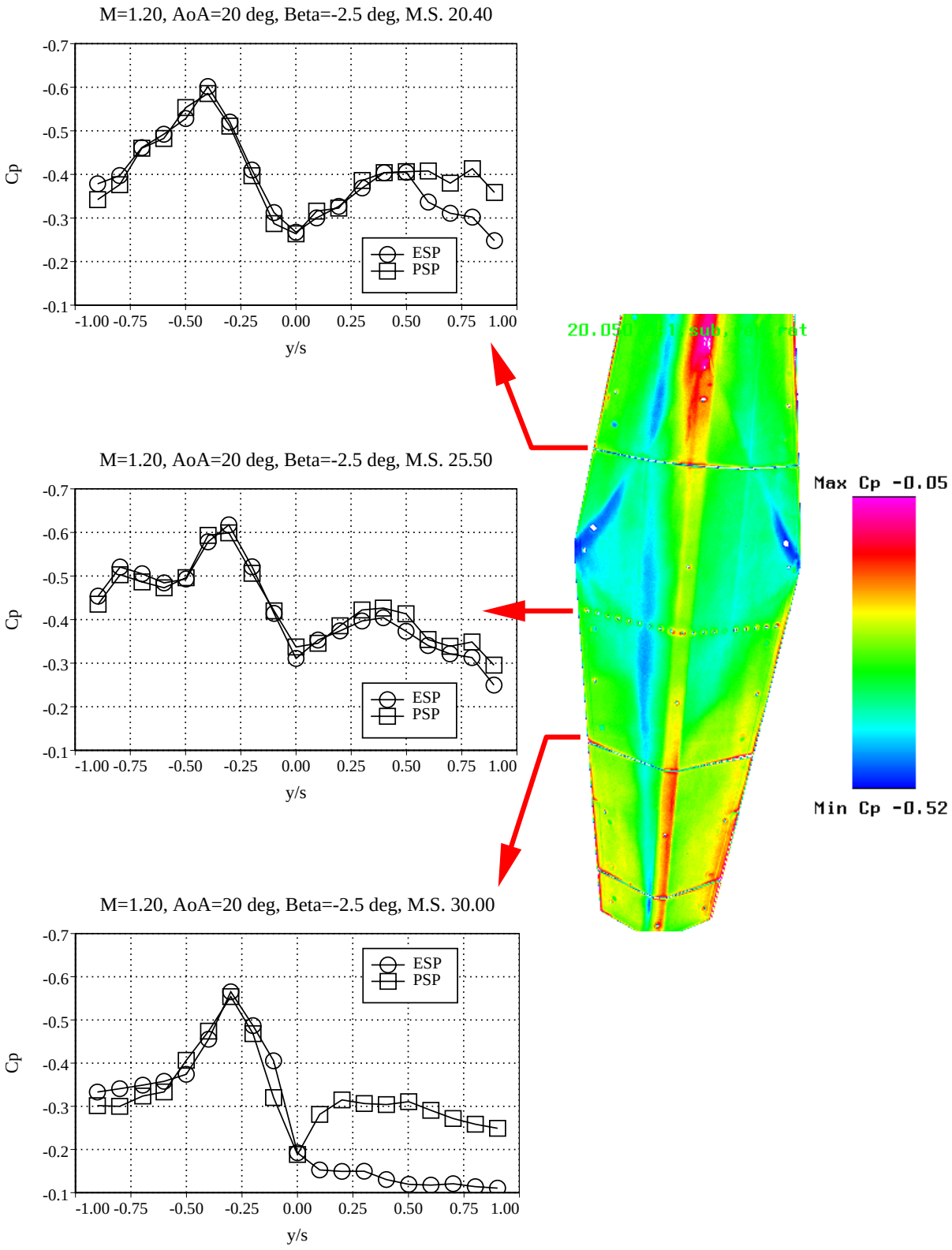

(g) $\alpha = 20$ degrees, $\beta = -2.5$ degrees.

Figure 11. Concluded.

REPORT DOCUMENTATION PAGE

Form Approved
OMB No. 0704-0188

1. REPORT DATE *(DD-MM-YYYY)*	2. REPORT TYPE	3. DATES COVERED *(From - To)*
01- 02 - 2004	Technical Memorandum	

4. TITLE AND SUBTITLE

Wind Tunnel Application of a Pressure-Sensitive Paint Technique to a Faceted Missile Model at Subsonic and Transonic Speeds

5a. CONTRACT NUMBER

5b. GRANT NUMBER

5c. PROGRAM ELEMENT NUMBER

6. AUTHOR(S)

Erickson, Gary E.

5d. PROJECT NUMBER

5e. TASK NUMBER

5f. WORK UNIT NUMBER

23-721-10-66

7. PERFORMING ORGANIZATION NAME(S) AND ADDRESS(ES)

NASA Langley Research Center
Hampton, VA 23681-2199

8. PERFORMING ORGANIZATION REPORT NUMBER

L-18327

9. SPONSORING/MONITORING AGENCY NAME(S) AND ADDRESS(ES)

National Aeronautics and Space Administration
Washington, DC 20546-0001

10. SPONSOR/MONITOR'S ACRONYM(S)

NASA

11. SPONSOR/MONITOR'S REPORT NUMBER(S)

NASA/TM-2004-212991

12. DISTRIBUTION/AVAILABILITY STATEMENT

Unclassified - Unlimited
Subject Category 02
Availability: NASA CASI (301) 621-0390 Distribution: Standard

13. SUPPLEMENTARY NOTES

An electronic version can be found at http://techreports.larc.nasa.gov/ltrs/ or http://ntrs.nasa.gov

14. ABSTRACT

A pressure-sensitive paint (PSP) technique was applied in a wind tunnel experiment in the NASA Langley Research Center 8-Foot Transonic Pressure Tunnel to quantify the vortex-induced surface static pressures on a slender, faceted missile model at subsonic and transonic speeds. Global PSP calibrations were obtained using an in-situ method featuring the simultaneous electronically-scanned pressures (ESP) measurements. Both techniques revealed the significant influence leading-edge vortices on the surface pressure distributions. The mean error in the PSP measurements relative to the ESP data was approximately 0.6 percent at M_∞=0.70 and 2.6 percent at M_∞=0.90 and 1.20. The vortex surface pressure signatures obtained from the PSP and ESP techniques were correlated with the off-surface vortex cross-flow structures obtained using a laser vapor screen (LVS) flow visualization technique. The on-surface and off-surface techniques were complementary, since each provided details of the vortex-dominated flow that were not clear or apparent in the other.

15. SUBJECT TERMS

Pressure-sensitive paint; Electronically-scanned pressures; Subsonic; Transonic; Supersonic; Missiles; Vortex flows; High angles of attack; Laser vapor screen; Flow physics; Flow visualization

16. SECURITY CLASSIFICATION OF:			17. LIMITATION OF ABSTRACT	18. NUMBER OF PAGES	19a. NAME OF RESPONSIBLE PERSON
a. REPORT	b. ABSTRACT	c. THIS PAGE			STI Help Desk (email: help@sti.nasa.gov)
					19b. TELEPHONE NUMBER *(Include area code)*
U	U	U	UU	45	(301) 621-0390